

# The Galaxy Clustering Crisis in Abundance Matching

Duncan Campbell<sup>1\*</sup>, Frank C. van den Bosch<sup>1</sup>, Nikhil Padmanabhan<sup>2,3</sup>, Andrew Zentner<sup>4</sup>, Johannes Lange<sup>1</sup>, Yao-Yuan Mao<sup>4</sup>, and Fangzhou Jiang<sup>5</sup>

<sup>1</sup>Department of Astronomy, Yale University, New Haven, CT 06511, USA

<sup>2</sup>Department of Physics, Yale University, New Haven, CT 06520, USA

<sup>3</sup>Yale Center for Astronomy and Astrophysics, Yale University, New Haven, CT 06520, USA

<sup>4</sup>Department of Physics and Astronomy & Pittsburgh Particle Physics, Astrophysics, and Cosmology Center (PITT PACC), University of Pittsburgh, Pittsburgh, PA 15260

<sup>5</sup>Racah Institute of Physics, The Hebrew University, Jerusalem 91904, Israel

Accepted XXX. Received YYY; in original form ZZZ

## ABSTRACT

Galaxy clustering on small scales is significantly under-predicted by sub-halo abundance matching (SHAM) models that populate (sub-)haloes with galaxies based on peak halo mass,  $M_{\text{peak}}$ . SHAM methods based on the peak maximum circular velocity,  $V_{\text{peak}}$ , have had much better success. The primary reason  $M_{\text{peak}}$  based models fail is the relatively low abundance of satellite galaxies produced in these models compared to those based on  $V_{\text{peak}}$ . Despite success in predicting clustering, simple  $V_{\text{peak}}$  based SHAM models have their own problems, and there is little theoretical reason to prefer  $V_{\text{peak}}$  over  $M_{\text{peak}}$  as a proxy for stellar mass. We identify three possible remedies that could save mass-based models. 1.) SHAM models require a significant population of “orphan” galaxies as a result of artificial disruption of sub-haloes in modern dark matter simulations, 2.) satellites must grow significantly after the time of accretion, and/or 3.) stellar mass is significantly affected by halo assembly history. Regardless of the particulars, we show that popular SHAM models based on  $M_{\text{peak}}$  cannot be correct as presented. Either  $V_{\text{peak}}$  truly is a better predictor of stellar mass, or SHAM models are missing vital component(s) that significantly affect galaxy clustering.

**Key words:** galaxies: halos – galaxies: evolution – galaxies: clustering

## 1 INTRODUCTION

The prevailing picture of galaxy formation is intricately tied to that of dark matter structure formation. The matter distribution of the Universe evolved from a relatively smooth state into a complex web of structure over  $\sim 14$  billion years. Within this web, small inhomogeneities evolved into extended, quasi-spherical, gravitationally bound objects called haloes. The build-up of structure proceeds hierarchically as smaller haloes are accreted into larger haloes, becoming substructures called sub-haloes. The potential wells of dark matter (sub-)haloes are the natural site for galaxies to form as baryons cool and condense into stars (Rees & Ostriker 1977; White & Rees 1978; Fall & Efstathiou 1980).

This general, albeit coarse, view of galaxy formation fits well with the premise of sub-halo abundance matching (SHAM). SHAM in its most simple form rests on the hypoth-

esis that all massive<sup>1</sup> (sub-)haloes host galaxies, all galaxies occupy (sub-)haloes, and there is a simple monotonic relation between galaxy mass and the mass of the (sub-)halo each galaxy occupies (Kravtsov et al. 2004; Conroy et al. 2006; Vale & Ostriker 2004). This approach relies on simulations of dark matter structure formation to provide robust statistical predictions for many properties of dark matter (sub-)haloes, e.g. halo mass functions, mass profiles, and the spatial clustering of haloes. By “populating” dark matter simulations with galaxies using the SHAM technique, the statistical predictions from simulations can be leveraged to constrain the galaxy-halo connection and make predictions for how galaxies form and evolve along with (sub-)haloes.

The stellar mass-halo mass (SMHM) relation is one of the most fundamental implications of SHAM. The SMHM relation at redshift  $\sim 0$  inferred using SHAM is consistent with HOD/CLF analysis (Yang et al. 2003; van den Bosch

\* E-mail: duncan.campbell@yale.edu

<sup>1</sup> above a limiting lower mass scale below which galaxy formation becomes inefficient

et al. 2003, 2007; Yang et al. 2013; Zu & Mandelbaum 2015a) and independent, more direct, measurements, e.g. galaxy-galaxy lensing, satellite kinematics, and the Tully-Fisher relation (Wang et al. 2006; More et al. 2009; Guo et al. 2010; Wang & Jing 2010; Moster et al. 2010; Behroozi et al. 2010; Mandelbaum et al. 2015; Desmond & Wechsler 2015; van Uitert et al. 2016). By extending this analysis to higher redshifts, the inferred evolution of the SMHM relation and the mass growth histories of haloes predicted by simulations provide constraints on the average stellar mass growth histories of galaxies that is consistent with the cosmic star-formation history of the Universe (Conroy & Wechsler 2009; Wang & Jing 2010; Yang et al. 2012; Moster et al. 2013; Behroozi et al. 2013c). An important finding of these studies is that the peak in star-formation efficiency shifts towards more massive haloes at earlier times.

The ability of SHAM to accurately predict the clustering of galaxies is more limited. In particular, the small scale clustering of galaxies remains difficult to fit. SHAM has only been shown to be consistent with galaxy clustering under one of two conditions: 1.) stellar mass is tied to the peak circular velocity of (sub-)haloes (or closely related quantities) (Reddick et al. 2013; Hearn et al. 2014; Lehmann et al. 2015), or 2.) the abundance of sub-haloes is treated as a free parameter (Wang et al. 2006; Wang & Jing 2010; Guo et al. 2010; Moster et al. 2010; Yang et al. 2012). This second approach relies on a population of “orphan” galaxies which have no identifiable sub-halo in a simulation. As we will show in this work, both of these assumptions are problematic. The assumption that stellar mass should be better correlated with maximum circular velocity over halo mass has not been robustly motivated. Furthermore, we show that models that make this assumption are at odds with previous work on the evolution of the SMHM relation. Orphan galaxies are difficult to reconcile with modern high resolution dark matter simulations which aim to resolve substructure. We summarize this state of affairs in Fig. 1. There is no published SHAM model which fits both galaxy clustering and the evolution of the stellar mass function using resolved substructure in a dark matter simulation without the addition of “orphan” galaxies.

The goal of this paper is threefold: to make explicit the tension between fitting galaxy clustering measurements and the evolution of the stellar mass function within the SHAM framework, to examine the successes and failures of SHAM models based on maximum circular velocity, and to evaluate mechanisms to alleviate the clustering crisis in models based on halo mass. The models and analysis in this paper utilize the framework and code base in `Halotools` (Hearn et al. 2016), an `Astropy` (The Astropy Collaboration et al. 2013) affiliated Python<sup>2</sup> package. We also make available all of the code and data products necessary to reproduce the figures and analysis in this paper<sup>3</sup>. Throughout, we scale all units by  $h = H_0/[100 \text{ km/s Mpc}^{-1}]$  where appropriate, and we use  $\log(x)$  to indicate the base 10 logarithm of  $x$ .

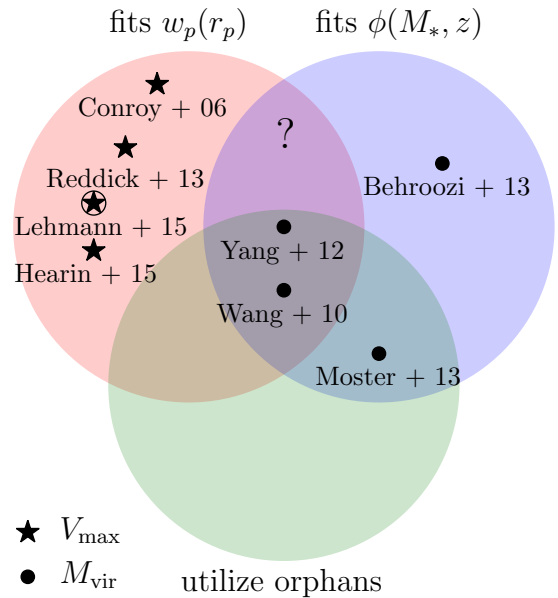


**Figure 1.** Venn diagram of selected SHAM models within three sets; those that fit the galaxy clustering,  $w_p(r_p)$  (upper left red region), those that fit the evolution of the galaxy stellar mass function,  $\phi(M_*, z)$  (upper right blue region), and those that utilize orphan galaxies (lower green region). Models marked with a circle are based on measures of halo mass,  $M_{\text{vir}}$ , including peak quantities. Models marked with a star are based on measures of halo maximum circular velocity,  $V_{\max}$ , including peak quantities, with the Lehmann et al. (2015) model falling somewhere in between. This paper focuses on the lack of models in the region marked with a “?”.

## 2 METHODS

### 2.1 Abundance Matching Models

SHAM, in its most simple form, assumes that the cumulative abundance of galaxies and haloes can be used to map galaxy properties uniquely onto (sub-)haloes. Using stellar mass,  $M_*$ , and a halo mass proxy  $\mathcal{M}$ , SHAM assumes:

$$N(> M_*) = N(> \mathcal{M}) \implies M_* = f(\mathcal{M}) \quad (1)$$

where  $f(\mathcal{M})$  is some monotonically increasing function. This maps the most massive galaxies to the most massive haloes. The function  $f(\mathcal{M})$  may be determined non-parametrically by matching the rank orders of galaxies and haloes. We refer to this method of SHAM as “rank order” abundance matching. However, we also consider another class of SHAM models where  $f(\mathcal{M})$  is parametrized. This introduces the possibility that the observed abundance of galaxies is not strictly matched; however, it is generally the goal of such models to preserve this characteristic. We consider these two types of models similar enough to be contained within the class of models we refer to as SHAM.

The predictions of SHAM are sensitive to the details of how it is implemented. Many halo properties have been examined in search of which “best” correlates with galaxy stellar mass or luminosity. It is generally found that “peak” values of mass-like properties, estimated over the history of the (sub-)halo, work best. Specifically, using the peak maxi-

<sup>2</sup> <http://www.python.org>

<sup>3</sup> [https://github.com/duncandc/Clustering\\_Crisis](https://github.com/duncandc/Clustering_Crisis)

113    mum circular velocity reproduces the clustering statistics of  
 114    galaxies most successfully (Conroy et al. 2006; Reddick et al.  
 115    2013). The difference between the peak values and current  
 116    values is most pronounced for sub-haloes, as sub-haloes are  
 117    subject to stripping processes which remove mass, while the  
 118    core of the sub-halo, which hosts a galaxy, is thought to  
 119    survive much longer (e.g. Behroozi et al. 2014a; van den  
 120    Bosch et al. 2016; Jiang & van den Bosch 2016; van den  
 121    Bosch 2016, and references therein). Implicit to the SHAM  
 122    algorithm is that the processes that set the properties of  
 123    central and satellite galaxies are independent of halo assem-  
 124    bly history. This assumption has been relaxed somewhat by  
 125    allowing satellites to either grow or lose stellar mass after  
 126    being accreted into a host-halo (Watson et al. 2012; Yang  
 127    et al. 2012; Behroozi et al. 2015) and is well motivated by  
 128    observations (Wetzel et al. 2013). Furthermore, the very dis-  
 129    tinction between host-haloes and sub-haloes is blurred by  
 130    the recognition that some haloes are accreted into a host-  
 131    halo, only for their orbit to take them outside their host’s  
 132    virial radius. For these “backsplash” haloes, it may be more  
 133    appropriate to treat them as sub-haloes likely to host galax-  
 134    ies that have properties more in common with traditionally  
 135    defined satellite galaxies (Mamon et al. 2004; Wetzel et al.  
 136    2014).

137    Below, we review a set of SHAM models and our method  
 138    of implementing each before examining the clustering pre-  
 139    dictions of each model in the following section. We provide  
 140    a summary of the models used in this paper in table 1.

### 141    2.1.1 Rank Order SHAM

142    The simplest implementation of SHAM maps galaxies into  
 143    (sub-)haloes by matching rank orders. Given a set of galax-  
 144    ies,  $M_* = \{M_{*i}\}$ , and (sub-)haloes,  $\mathcal{M} = \{\mathcal{M}_j\}$ , of the same  
 145    size, this method proceeds by calculating the ranks of each:

$$\begin{aligned} n_i^{\text{gal}} &= \mathcal{R}(M_*) \\ n_j^{\text{halo}} &= \mathcal{R}(\mathcal{M}) \end{aligned} \quad (2)$$

146    where the  $\mathcal{R}()$  function returns the ordinal ranks. Each  
 147    galaxy is then assigned to a (sub-)halo with the equivalent  
 148    rank, i.e.  $n_i^{\text{gal}} = n_j^{\text{halo}}$ . We consider two rank order SHAM  
 149    models in this paper, one based on  $M_{\text{peak}}$  and one on  $V_{\text{peak}}$ .  
 150    As shorthand, we refer to these models as “RM” and “RV”,  
 151    respectively.

152    Given a set of galaxies and haloes, this mapping is deter-  
 153    ministic. However, the assumption of perfect rank ordering  
 154    with respect to the cumulative distribution can be relaxed,  
 155    allowing for stochasticity in the mapping and resulting in  
 156    a probabilistic relation between stellar mass and halo mass,  
 157     $P(M_*|\mathcal{M})$ . There are various methods used in the literature  
 158    to add scatter to this relation while maintaining agreement  
 159    with an observed stellar mass function. One may attempt to  
 160    deconvolve the stellar mass function from the scatter model  
 161    such that, after solving for eq. (1) with this deconvolved  
 162    function and applying the scatter model, the new stellar  
 163    mass function is consistent with the observed function (e.g.  
 164    Behroozi et al. 2010). Another option is to manually add  
 165    scatter to the stellar masses used in abundance matching,  
 166    re-ranking on the new values to perform the matching, and  
 167    iteratively solving for a solution that results in the desired  
 168    amount of scatter in the SMHM relation (e.g. Hearin et al.

Table 1. Summary SHAM models used in this paper

name	reference	description
RM	–	rank order SHAM on $M_{\text{peak}}$
RV	–	rank order SHAM on $V_{\text{peak}}$
M13	Moster et al. (2013)	evolving SMHM model
B13	Behroozi et al. (2013c)	evolving SMHM model
Y12	Yang et al. (2012)	evolving SMHM model

169    2013). A third option is to parametrize the SMHM relation  
 170    and fit for the parameters which result in a stellar mass  
 171    function that is consistent with an observed function after  
 172    populating a dark matter simulation. We will examine this  
 173    type of model in the following sections.

174    We do not go through the additional step of adding  
 175    scatter to our RM and RV models, as scatter in the SMHM  
 176    relation generally decreases the strength of the clustering  
 177    signal for massive galaxies ( $M_* > 10^{11} h^{-2} M_\odot$ ) with little  
 178    effect at lower masses (Tinker et al. 2016), and this work  
 179    focuses on the decrement in clustering signal for samples of  
 180    less massive galaxies.

### 181    2.1.2 Moster et al. (2013) SHAM

182    Moster et al. (2013) parametrize the SMHM relation as a  
 183    function of halo mass and redshift to account for evolution.  
 184    Furthermore, they assume the stellar mass of satellite galax-  
 185    ies is determined by the mass of the sub-halo at the time of  
 186    its accretion into a more massive host-halo for the first time.  
 187    The functional form is given by:

$$\frac{\langle M_* | \mathcal{M} \rangle_{\text{med}}(a)}{\mathcal{M}} = 2N \left[ \left( \frac{\mathcal{M}}{M_1} \right)^{-\beta} + \left( \frac{\mathcal{M}}{M_1} \right)^\gamma \right]^{-1} \quad (3)$$

188    where  $\langle \rangle_{\text{med}}$  indicates the median. The evolution of the pa-  
 189    rameters is given by:

$$\log[M_1(a)] = M_{10} + M_{11}(1-a) \quad (4)$$

$$N(a) = N_{10} + N_{11}(1-a) \quad (5)$$

$$\beta(a) = \beta_{10} + \beta_{11}(1-a) \quad (6)$$

$$\gamma(a) = \gamma_{10} + \gamma_{11}(1-a) \quad (7)$$

190    where the scale factor is either the instantaneous scale factor,  
 191    or the one at the time of accretion:

$$a = \begin{cases} a & \text{if host-halo} \\ a_{\text{acc}} & \text{if sub-halo} \end{cases} \quad (8)$$

192    and  $\mathcal{M}$  is the instantaneous mass or the mass at accretion,  
 193     $M_{\text{acc}}$ , for sub-haloes. Scatter in the SMHM relation is mod-  
 194    elled as a fixed log-normal with  $\sigma \approx 0.18$ .

195    Moster et al. (2013) find the best fit parameters for  
 196    equation (3) that reproduce the stellar mass function at var-  
 197    ious redshifts between 0 and  $\sim 4$ . They also show that the  
 198    implied star-formation rates of galaxies given the growth  
 199    history of the (sub-)haloes in their simulation is consistent  
 200    with the cosmic star-formation rate density. The parame-  
 201    ters were constrained using the Millennium simulation with  
 202    (sub-)haloes defined as spherical over-densities (SO) with  
 203    mean internal density 200 times the critical density of the  
 204    universe,  $M_{200c}$ . As shorthand, we will refer to this model

as “M13”. The parameters in this model were constrained in M13 by fitting to the stellar mass function at multiple epochs between  $z=0$ -4. The parameter values used in this paper are taken directly from Moster et al. (2013) and listed in table 2.

### 2.1.3 Behroozi et al. (2013) SHAM

Behroozi et al. (2013c) make similar assumptions as M13 but utilize a different parametrization given by:

$$\log[\langle M_* | \mathcal{M} \rangle_{\text{med}}(a)] = \log(\epsilon M_1) + f(\log(\mathcal{M}/M_1)) - f(0) \quad (9)$$

where,

$$f(x) = -\log(10^{\alpha x} + 1) + \delta \frac{[\log(1 + \exp[x])]^\gamma}{1 + \exp(10^{-x})} \quad (10)$$

and where  $\mathcal{M} = M_{\text{peak}}$ . The parameters evolve with redshift as:

$$\nu(a) = e^{-4a^2} \quad (11)$$

$$\log[M_1(a)] = M_{10} + \nu [M_{1,a}(a-1) + M_{1,z}(z)] \quad (12)$$

$$\log[\epsilon(a)] = \epsilon_0 + \nu [\epsilon_a(a-1) + \epsilon_z(z)] + \epsilon_{a,2}(a-1) \quad (13)$$

$$\alpha(a) = \alpha_0 + \nu [\alpha_a(a-1)] \quad (14)$$

$$\delta(a) = \delta_0 + \nu [\delta_a(a-1) + \delta_z(z)] \quad (15)$$

$$\gamma(a) = \gamma_0 + \nu [\gamma_a(a-1) + \gamma_z(z)] \quad (16)$$

When fitting their model, Behroozi et al. (2013c) also allow the scatter in the SMHM relation to vary as a function of redshift. The variation found is consistent with no variation (constant over cosmic time), so we neglect the small variation in the best fit model and use a constant non-varying scatter. We have checked that including this variation has no appreciable effect on our conclusions. As shorthand, we will refer to this model as “B13”. B13 constrained the parameters of this model by fitting the stellar mass function at multiple epochs, specific star-formation rates, and the cosmic star-formation history between  $z=0$ -8. The values used in this paper are taken directly from Behroozi et al. (2013c) and listed in table 2.

### 2.1.4 Yang et al. (2012) SHAM

Yang et al. (2012) take a different approach than M13 and B13. They allow for evolution with redshift in a similar manner, but additionally allow satellites to grow or lose mass after the time of accretion. The SMHM relation for central galaxies is:

$$\langle M_{*,\text{cen}} | \mathcal{M} \rangle_{\text{med}}(z) = M_0 \frac{(\mathcal{M}/M_1)^{\alpha+\beta}}{(1 + \mathcal{M}/M_1)^\beta} \quad (17)$$

where  $\mathcal{M} = M_{180b}$ , and the parameters<sup>4</sup> evolve with redshift as:

$$\log[M_0(z)] = M_{01} + \gamma_1 z \quad (18)$$

$$\log[M_1(z)] = M_{11} + \gamma_2 z \quad (19)$$

$$\alpha(z) = \alpha_0 + \gamma_3 z \quad (20)$$

$$\log[\beta(z)] = \log(\beta_0) + \gamma_4 z + \gamma_5 z^2 \quad (21)$$

<sup>4</sup> We have altered the naming scheme somewhat to be more consistent with the other models.

The mean stellar mass of satellites is determined by interpolating between the stellar mass a satellite would have had at the time of accretion and the stellar mass of a central galaxy with the same halo mass as the satellite at accretion. This value is determined by a single parameter,  $c$ :

$$\langle M_{*,\text{sat}}(z, z_{\text{acc}}) \rangle = (1 - c) \langle M_{*,\text{cen}} | \mathcal{M}_{\text{acc}} \rangle(z_{\text{acc}}) + c \langle M_{*,\text{cen}} | \mathcal{M} \rangle(z) \quad (22)$$

where  $\mathcal{M}_{\text{acc}}$  is the halo mass proxy at the time of accretion for the sub-halo. The case where  $c = 0$  corresponds to no growth (or mass loss) since the time of accretion. The case where  $c = 1$  corresponds to using the same SMHM relation for centrals and satellites at all redshifts.

Apart from the parametrization of the SMHM relation and its evolution, the original implementation of Yang et al. (2012) differs significantly from the previous two models in that it uses a fully analytical halo+sub-halo model for abundances, sub-halo profiles, and halo bias. We take a different approach and use the SMHM relation of the model and apply it directly to a simulation, side-stepping the need to analytically model these components. Multiple fits were performed in Yang et al. (2012). We use the parameter constraints determined by fitting the stellar mass function at multiple epochs ( $z=0$ -5) as well as the conditional stellar mass function at  $z \sim 0$ . This set of parameters was also shown to fit galaxy clustering observations well at  $z \sim 0$ . The values used in this paper are listed in table 2, specifically these are taken from Table 4 (ID=4) in Yang et al. (2012). As shorthand, we will refer to this model as “Y12”.

## 2.2 Dark Matter Simulations

We build our mock galaxy catalogues using the Bolshoi (Klypin et al. 2011) simulation output at  $z=0.0$ . The Bolshoi simulation follows the evolution of  $2048^3$  dark matter particles using the Adaptive Refinement Tree (ART) code (Kravtsov, Klypin & Khokhlov 1997) in a flat  $\Lambda$ CDM cosmology with parameters  $\Omega_{\text{m},0} = 1 - \Omega_{\Lambda,0} = 0.27$ ,  $\Omega_{\text{b},0} = 0.0469$ ,  $n_s = 0.95$ ,  $\sigma_8 = 0.82$ , and  $h = 0.7$  (hereafter “Bolshoi cosmology”). The box size of the Bolshoi simulation is  $L_{\text{box}} = 250 h^{-1}\text{Mpc}$ , with a dark matter particle mass of  $m_{\text{p}} = 1.35 \times 10^8 h^{-1}\text{M}_\odot$ .

(Sub-)haloes are found using the phase-space halo finder ROCKSTAR (Behroozi et al. 2013a,b), which uses adaptive, hierarchical refinement of friends-of-friends groups in six phase-space dimensions and one time dimension. As demonstrated in Knebe et al. (2011, 2013), this results in a very robust tracking of (sub-)haloes (also see van den Bosch & Jiang 2014). Haloes in this catalogue are defined to be spherical volumes centred on a local density peak (SO hereafter), such that the average density inside the sphere is  $\bar{\rho}_{\text{h}}(z) = \Delta_{\text{vir}}(z)\rho_{\text{m}}(z)$ . Here  $\rho_{\text{m}}(z) = \Omega_{\text{m}}(z)\rho_{\text{crit}}(z)$ , where  $\rho_{\text{crit}}(z) = 3H(z)^2/8\pi G$  is the critical energy density of the Universe, and  $\Delta_{\text{vir}}(z)$  is given by a fitting function (Bryan & Norman 1998):

$$\Delta_{\text{vir}}(z) = [18\pi^2 - 82\Omega_{\Lambda}(z) - 39\Omega_{\Lambda}^2(z)]\Omega_m^{-1} \quad (23)$$

For the Bolshoi cosmology,  $\Delta_{\text{vir}}(z=0) \simeq 360$ . The radius of each such sphere defines the virial radius  $R_{\text{vir}}$  of the halo, which is related to the mass of the halo via  $M_{\text{vir}} = (4/3)\pi R_{\text{vir}}^3 \bar{\rho}_{\text{h}}$ . Additionally, sub-haloes in this catalogue are distinct, self-bound structures whose centre is

**Table 2.** Parameter values used for the evolving SHAM models presented in this paper. Mass parameters in M13 and B13 are scaled to  $h=0.7$ , while in Y12,  $h=1$  as is the practice in the rest of this paper. We use the parameters as is, and scale the output stellar masses to  $h=1$ .

model	parameter	value	uncertainty
M13	$M_{10}$	11.590	$\pm 0.236$
M13	$M_{11}$	1.195	$\pm 0.353$
M13	$N_{10}$	0.0351	$\pm 0.0058$
M13	$N_{11}$	-0.0247	$\pm 0.0069$
M13	$\beta_{10}$	1.376	$\pm 0.153$
M13	$\beta_{11}$	-0.826	$\pm 0.225$
M13	$\gamma_{10}$	0.608	$\pm 0.059$
M13	$\gamma_{11}$	0.329	$\pm 0.173$
B13	$M_{10}$	11.514	$\pm^{0.053}_{0.009}$
B13	$M_{1,a}$	-1.793	$\pm^{0.315}_{0.330}$
B13	$M_{1,z}$	-0.251	$\pm^{0.02}_{0.125}$
B13	$\epsilon_0$	-1.777	$\pm^{0.138}_{0.166}$
B13	$\epsilon_a$	-0.006	$\pm^{0.113}_{0.361}$
B13	$\epsilon_z$	-0.000	$\pm^{0.003}_{0.104}$
B13	$\epsilon_{a,2}$	-0.119	$\pm^{0.061}_{0.012}$
B13	$\alpha_0$	-0.119	$\pm^{0.061}_{0.012}$
B13	$\alpha_a$	-0.119	$\pm^{0.061}_{0.012}$
B13	$\delta_0$	-1.777	$\pm^{0.133}_{0.146}$
B13	$\delta_a$	-0.006	$\pm^{0.113}_{0.361}$
B13	$\delta_z$	-0.000	$\pm^{0.003}_{0.104}$
B13	$\gamma_0$	-1.777	$\pm^{0.138}_{0.166}$
B13	$\gamma_a$	-0.006	$\pm^{0.113}_{0.361}$
B13	$\gamma_z$	-0.000	$\pm^{0.003}_{0.104}$
Y12	$M_{01}$	10.36	$\pm^{0.05}_{0.06}$
Y12	$M_{11}$	11.06	$\pm^{0.08}_{0.15}$
Y12	$\alpha_0$	0.27	$\pm^{0.01}_{0.01}$
Y12	$\beta_0$	4.34	$\pm^{0.96}_{0.52}$
Y12	$\gamma_1$	-0.96	$\pm^{0.13}_{0.19}$
Y12	$\gamma_2$	-0.23	$\pm^{0.06}_{0.05}$
Y12	$\gamma_3$	-0.41	$\pm^{0.07}_{0.08}$
Y12	$\gamma_4$	-0.11	$\pm^{0.05}_{0.08}$
Y12	$\gamma_5$	0.01	$\pm^{0.05}_{0.07}$
Y12	$c$	1.0	—

found within the virial radius of a more massive host-halo. For each (sub-)halo, the maximum circular velocity is defined as:  $V_{\max} \equiv \text{Max}[GM(< r)/r]$ , where  $M(< r)$  is the mass enclosed within a distance  $r$  of the (sub-)halo centre.

From this catalogue we construct our mocks primarily using three values for each (sub-)halo:  $M_{\text{peak}}$ ,  $V_{\text{peak}}$ , and  $z_{\text{acc}}$ .  $M_{\text{peak}}$  is defined as the peak virial mass a (sub-)halo achieves over its history. In our halo catalogues, we retain all (sub-)haloes that obtained a peak mass greater than fifty times the particle mass,  $m_p$ .  $z_{\text{acc}}$  is roughly the redshift a sub-halo is first accreted.  $V_{\text{peak}}$  is the peak value of the maximum circular velocity,  $V_{\max}$ , a (sub-)halo obtains over the course of its history. A detailed description of how each of these quantities is calculated can be found in Appendix A.

### 2.3 Populating Simulations

We build mock galaxy catalogues using the models and simulation described in the previous sections. For the rank order SHAM models, RM and RV, we use the triple piece-wise

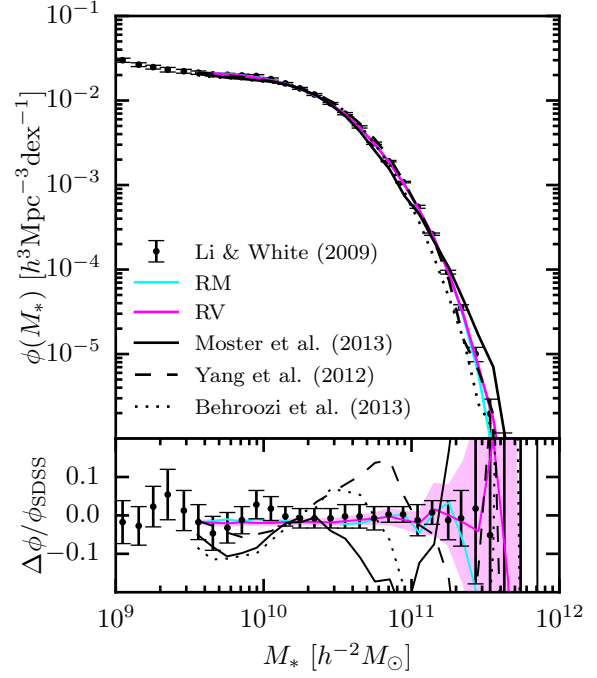


**Figure 2.** The stellar mass function of a mock realization of each model is plotted (lines). For comparison we show the stellar mass function in SDSS as measured by Li & White (2009) as points with error bars. The lower panel shows the residuals with respect to the triple Schechter fit from Li & White (2009). We show the  $\pm 1\sigma$  error on the model prediction for the RV as the shaded magenta region model as an example [DC: still adjusting this to bring each model into better agreement]

Schechter function fit to the stellar mass function,  $\phi_{\text{SDSS}}$ , from Li & White (2009, LW09 hereafter). This stellar mass function is based on a complete sample of galaxies from SDSS and assumes a universal Chabrier (2003) initial mass function (IMF). We integrate the stellar mass function to get the cumulative stellar mass function:

$$N(> M_*) = V \int_{M_*}^{\infty} \phi_{\text{SDSS}}(M') dM' \quad (24)$$

where  $V$  is the volume of the simulation being populated. We then normalize by the total number of galaxies above the threshold,  $N_{\text{lim}} = N(> 10^{9.5} h^{-2} M_\odot)$ , to get  $F(M_*) = N(> M_*)/N_{\text{lim}}$ , the cumulative probability distribution of galaxies as a function of stellar mass. We then draw from this distribution  $N_{\text{lim}}$  times using the inverse transform sampling method. In this way, each sampling is a Monte Carlo (MC) realization of the stellar mass function in the simulation volume. (Sub-)haloes are then populated by matching rank orders between stellar mass and (sub-)halo mass such that the most massive (sub-)haloes receive the most massive galaxies.

The parametrized SMHM models are populated in a different manner. The population of the simulation is a MC realization which begins by calculating the mean stellar mass

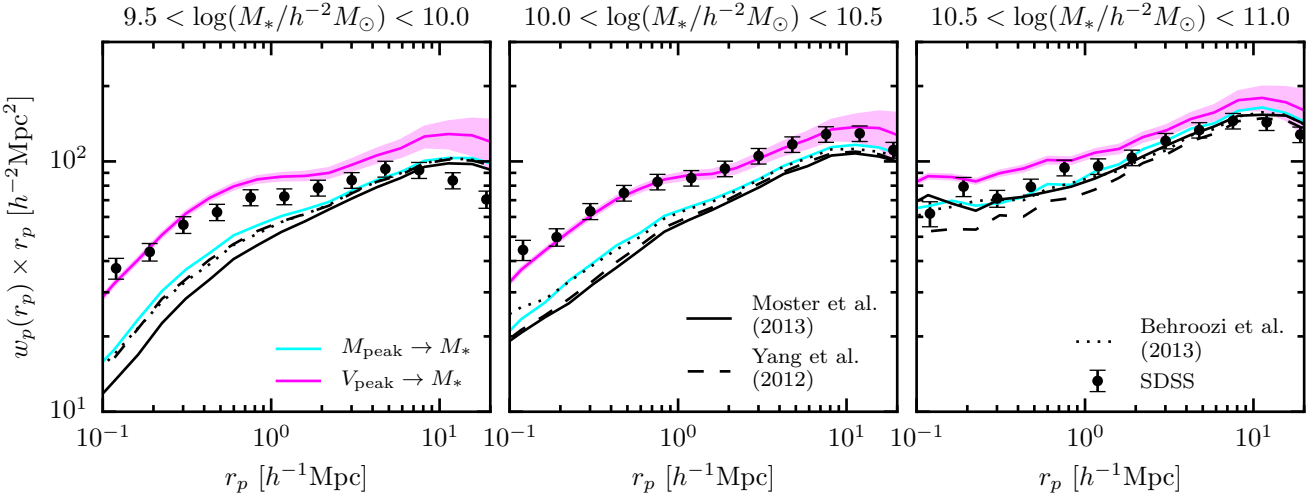


**Figure 3.** The projected correlation function,  $w_p$ , is plotted in three stellar mass bins for five SHAM models (lines). As an example, we show the  $\pm 1\sigma$  error on the model prediction for the RV model as the shaded magenta region. For comparison, we plot the projected correlation function of galaxies in SDSS as measured by Yang et al. (2012) as points with error bars.

for each (sub-)halo and adding random scatter:

$$\log[M_*(M_{\text{peak}}, a_{\text{acc}})] = \log[\langle M_* | M_{\text{peak}} \rangle(a_{\text{acc}})] + \mathcal{N}(0, \sigma_{\log(M_*)}) \quad (25)$$

where  $\mathcal{N}(0, \sigma_{\log(M_*)})$  is a random variable drawn from a normal distribution with mean 0 and a fixed log-scatter given by  $\sigma_{\log(M_*)}$ . We use  $M = M_{\text{peak}}$  for all the models, but we confirm that using  $M_{\text{acc}}$  instead does not significantly affect our results.

This step is slightly complicated by the fact that each model's parameters were tuned using different halo mass definitions,  $M_{\Delta_{\text{halo}}}$ . The M13 model uses  $M_{200c}$ , Y12 uses  $M_{180b}$ , and B13 uses  $M_{360b}$ . As described in the previous section, our halo catalogue defines haloes as SO with masses given by  $M_{360b}$ . We use  $M_{\text{peak}}$  directly for the B13 model, and for the M13 and Y12 models we convert  $M_{\text{peak}}$  from  $M_{360b}$  masses to the appropriate version for each model using a fitting function,  $f_{\text{conv}}$  (see appendix C in Hu & Kravtsov 2003). In the conversion we assume all haloes are fit by an NFW profile (Navarro et al. 1997) and use halo concentrations measured by ROCKSTAR at the time  $M_{\text{peak}}$  is achieved,  $c_{\text{peak}}$ .

$$M'_{\text{peak}} = f_{\text{conv}}(M_{\text{peak}}, c_{\text{peak}}, \Delta_{\text{halo}}) \quad (26)$$

Furthermore, each of the evolving models was tuned using observations based on different methods of determining stellar mass. We apply a simple set of conversions in order to homogenize the stellar masses to a single system as described in Appendix B. We show the stellar mass function for a mock based on each model in Fig. 2. The stellar mass functions in each mock vary by up to  $\sim 0.2$  dex from our fiducial stellar mass function used to create the RM and RV mocks. This is the result of each model being tuned with differing:

- (i) stellar mass functions,  $\phi(M_*, z)$
- (ii) halo mass definitions/(sub-)halo finder
- (iii) cosmologies

(iv) simulations which are subject to cosmic variance

While in principle each model could be re-fit using the same stellar mass function(s) and simulation, that is beyond the scope of this paper. We check that simple alterations to the parameters of each model which bring each into better agreement with the LW09 stellar mass function do not have a significant effect on the clustering signal predictions presented in §3. Given this, and the complexity involved in re-fitting each model, we use the parameters as they are quoted in each paper (and reproduced in table 2, with only minor alterations as discussed in the sections above).

### 3 CLUSTERING

In this section we present the galaxy clustering predictions of each SHAM model described in the previous section. We calculate the projected correlation function for each model, defined as:

$$w_p(r_p) = 2 \int_0^{r_{\parallel \max}} \xi(r_{\parallel}, r_p) dr_{\parallel} \quad (27)$$

where  $r_{\parallel}$  is the separation parallel to the line-of-sight (LOS),  $r_p$  the separation perpendicular to the LOS, and  $\xi$  is the two-point correlation function. We set  $r_{\parallel \max} = 40 h^{-1} \text{Mpc}$  to mimic equivalent measurements made using SDSS galaxies (Yang et al. 2012). The choice of  $r_{\parallel \max}$  is a balance between minimizing the contribution of redshift space distortions to the measurement, and maximizing the signal to noise in the measurement (Padmanabhan et al. 2007; van den Bosch et al. 2013).

We assume the “distant observer” approximation when calculating  $w_p$ . We approximate the LOS direction to a galaxy as  $\hat{z}$ , and take the plane-of-the-sky to be coincident with the x-y plane of the simulation box. This assumption holds when the distance between the “observer” and galaxies is much larger than the maximum separation between galax-

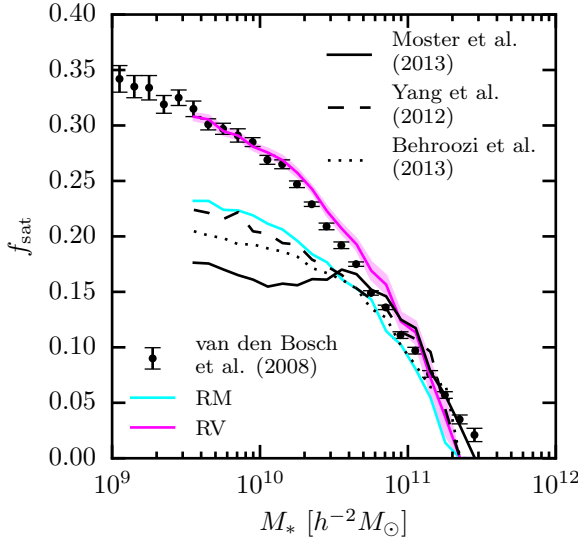


**Figure 4.** The satellite fraction as a function of stellar mass is plotted for SHAM model as lines. The models are RM (solid cyan), RV (solid magenta with the shaded region showing  $\pm 1\sigma$  error on the model prediction), M13 (solid black), Y12 (dashed), and B13 (dotted). For comparison, we show the satellite fraction as inferred by van den Bosch et al. (2008) using a galaxy group catalogue of SDSS galaxies.

ies which enters the calculation for a given statistic. Since we measure  $w_p$  only out to 20 Mpc, this is a safe approximation.

Any residual effects should be minimal because we also place galaxies in each mock in “redshift space”. Galaxies are assigned the peculiar velocity of the (sub-)halo which they occupy,  $\vec{v}_{\text{pec}}$ . The cosmological redshift is calculated using the z-position of the galaxy in the mock. The “observed” distance to a galaxy is then:

$$z' = [z_{\text{cosmo}} + (v_{\text{pec},z}/c) \times (1 + z_{\text{cosmo}})] c/H_0 \quad (28)$$

where we additionally account for the periodic boundary conditions of the simulation. We estimate jackknife errors on  $w_p$  by sub-dividing the simulation box into 27 equal cubic sub-volumes.

The projected correlation functions for each model calculated in three stellar mass bins as described above are shown in Fig. 3. For comparison, we show the corresponding measurement made on a galaxy sample in SDSS (“Mass-limit” sample in Yang et al. 2012). The difference between the clustering signal predictions of each SHAM model and observations is striking. Each halo mass-based models<sup>5</sup> severely under-predicts the clustering signal in the two least massive bins (left two panels), while the RV model, based on  $V_{\text{peak}}$ , if anything, slightly over-predicts the signal. On the other hand, all the models considered here roughly predict an accurate clustering signal consistent with observations in the most massive stellar mass bin (right panel).

<sup>5</sup> As a short-hand, we will frequently refer to the RM, M13, B13, and Y12 models as “mass-based models”.

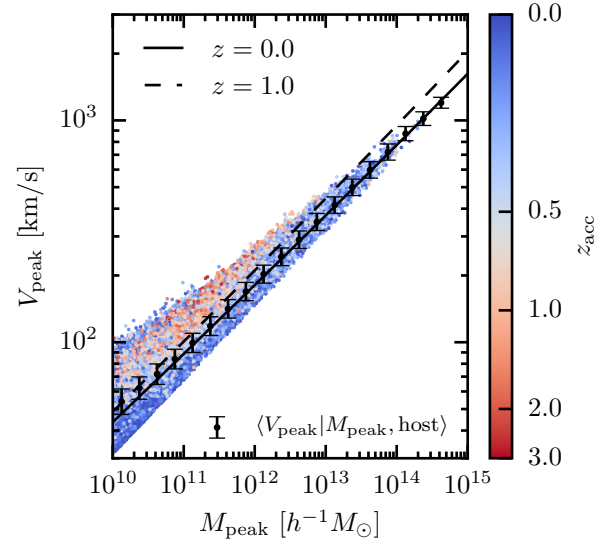


**Figure 5.** The relation between  $M_{\text{peak}}$  and  $V_{\text{peak}}$  is plotted for all sub-haloes in the Bolshoi simulation at  $z=0$ , colour-coded according to the redshift at the time of accretion,  $z_{\text{acc}}$ . For host-haloes, the median  $V_{\text{peak}}$  in 0.25 dex bins of  $M_{\text{peak}}$  is plotted as black points with error bars indicating the log-normal scatter. The solid line shows the median  $V_{\text{peak}}$  relation in eq. 29 at  $z=0$ . The dashed line shows the same relation at  $z=1$ . Sub-haloes have systematically higher values of  $V_{\text{peak}}$  than host-haloes at fixed  $M_{\text{peak}}$ .

#### [add discussion of cosmic variance in the SDSS measurements]

The success of the RV model is consistent with findings by Reddick et al. (2013) who show that SHAM based on  $V_{\text{peak}}$  most closely matches galaxy clustering observations in SDSS, while all other halo properties under-predict the signal. We confirm that result here; furthermore, we show that more complicated evolving SMHM models based on  $M_{\text{peak}}$  do not alleviate the problem. In fact, evolution seems to exacerbate the clustering decrement of  $M_{\text{peak}}$  based SHAM as evidenced by the RM model producing the strongest clustering signal amongst the mass-based models. The remainder of this paper examines why these models fail to produce strong enough clustering, why the RV model (and similar models) succeeds, and possible solutions to “save” mass-based SHAM models (under the assumption these models are worth saving).

## 4 THE $V_{\text{PEAK}}$ MIRACLE

In this section, we examine the origin of the success of  $V_{\text{peak}}$  based SHAM models. By comparing the differences in  $V_{\text{peak}}$  and  $M_{\text{peak}}$  based models, we identify the culprit(s) in the failure of the mass-based models to match observational clustering measurements. We also discuss some reasons to prefer mass-based models over  $V_{\text{peak}}$  based models.

443 **4.1 Satellite Fraction**

444 Where clustering is under-predicted, the problem is most  
 445 severe at small scales ( $< 1 h^{-1} \text{Mpc}$ ). This is a strong indica-  
 446 tion that the culprit is satellite galaxies, or more precisely,  
 447 a lack of satellite galaxies in the mass-based SHAM mocks.  
 448 With this in mind, we examine the satellite fraction,  $f_{\text{sat}}$ ,  
 449 in each mock in Fig. 4. The RV model has a larger satellite  
 450 fraction,  $\sim 27\%$ , relative to the other models which are be-  
 451 low  $\sim 22\%$ . Comparing the clustering signals in Fig. 3 with  
 452 the satellite fractions in Fig. 4 shows that there is a nearly  
 453 one-to-one correspondence between the clustering strength  
 454 on small scales and  $f_{\text{sat}}$  of each model. Furthermore, the  
 455 satellite fractions between the models do not diverge un-  
 456 til approximately  $5 \times 10^{10} h^{-2} M_{\odot}$ , above which the models  
 457 largely agree with the clustering results. Considering this, it  
 458 may be more appropriate to restate the under-prediction of  
 459 galaxy clustering in these models as an underproduction of  
 460 satellite galaxies.

461 **4.2 Why does  $V_{\text{peak}}$  SHAM have increased  $f_{\text{sat}}$ ?**

462 As can be seen in Fig. 5,  $V_{\text{peak}}$  and  $M_{\text{peak}}$  are highly cor-  
 463 related properties with small scatter,  $\sigma_{\log(V_{\text{peak}})} \sim 0.05$  at  
 464 fixed mass for host-haloes. Additionally, sub-haloes have on  
 465 average larger  $V_{\text{peak}}$  than host-haloes of equal  $M_{\text{peak}}$ . The  
 466 reasoning behind this difference between host-haloes and  
 467 sub-haloes is straight forward. For an NFW profile,  $V_{\text{max}}$  is  
 468 an increasing function of the halo mass and concentration,  
 469  $V_{\text{max}} = f(m_{\text{vir}}, c_{\text{vir}})$  (see eq. 6 in van den Bosch et al. 2014).  
 470 Furthermore, it is a robust prediction of  $\Lambda$ CDM dark matter  
 471 simulations that halo concentration correlates with halo for-  
 472 mation time,  $\langle z_f \rangle = f(m_{\text{vir}}, c_{\text{vir}})$  (e.g. Wechsler et al. 2002).  
 473 Finally, because  $M_{\text{peak}}$  occurs before accretion for sub-haloes  
 474 and near  $z=0$  for host-haloes, sub-haloes generally have ear-  
 475 lier formation times at fixed  $M_{\text{peak}}$ .

476 Given this, and using the concentration-mass-redshift  
 477 relation from Macciò et al. (2009). We devise a description  
 478 for the median  $M_{\text{peak}} - V_{\text{peak}}$  relation given by:

$$\langle V_{\text{peak}} \rangle(M_{\text{peak}}, z) = 1.1 \times V_{\text{max}}(M_{\text{peak}}, z) \quad (29)$$

479 where we include the factor of 1.1 to account for the fact that  
 480 the average peak maximum circular velocity is  $\sim 10\%$  higher  
 481 than  $V_{\text{max}}$  (Behroozi et al. 2014b). We show this relation at  
 482  $z = 0$  (solid line) and at  $z = 1.0$  (dashed line) in Fig. 5.

483 It is the correlated scatter in  $V_{\text{peak}}$  at fixed  $M_{\text{peak}}$  which  
 484 is responsible for the difference in the satellite fractions be-  
 485 tween the RV and RM models. By populating (sub-)haloes  
 486 by their rank on  $V_{\text{peak}}$ , more sub-haloes will be populated  
 487 than would have been had  $M_{\text{peak}}$  instead been utilized for  
 488 any given stellar mass threshold sample. This same reason-  
 489 ing carries over to the other mass-based models.

490 **4.3 The Evolving Relation between  $M_*$  and  $M_{\text{halo}}$**

491 Here we compare the RV model to the other models by ex-  
 492 amining the relation between stellar mass and halo mass that  
 493 arises in each model, in the RV model by correlation between  
 494  $V_{\text{peak}}$  and  $M_{\text{peak}}$ , and in the other models by design. In the  
 495 top panel of Fig. 6, we examine the relation between stellar  
 496 mass and  $M_{\text{peak}}$  for individual galaxies in the RV mock. Be-  
 497 yond the ubiquitous shape of the SMHM relation, the most

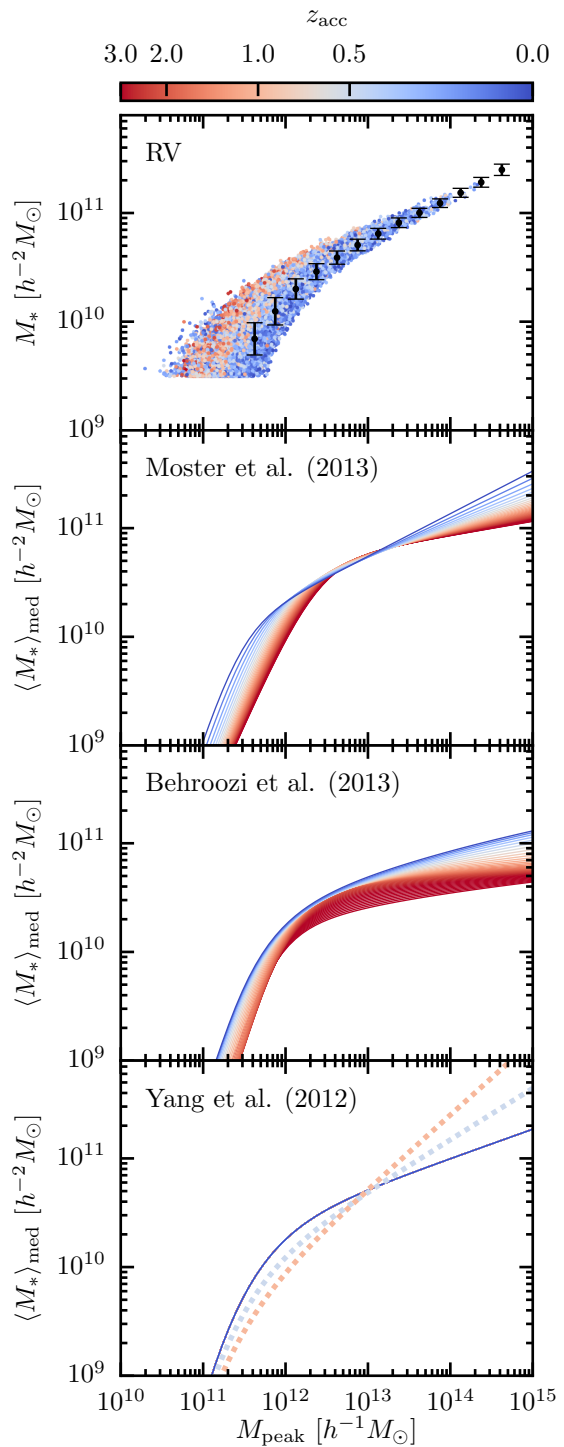


**Figure 6.** The SMHM relation in the RV model and the three evolving SHAM models. From top to bottom, the panels show RV, M13, B13, and Y12. For each model, the SMHM relation is shown at  $z=0$  as a function of the redshift of accretion,  $z_{\text{acc}}$ , for satellites. The top panel shows the mean stellar mass and scatter of central galaxies as points with error bars with satellites shown as colour-coded points. For the remaining panels, the analytic functions are shown. For these models, the relation for centrals is shown with  $x_{\text{acc}}$  set to 0.0. The dotted lines in the bottom panel give the relation for central galaxies at  $z=1$  and  $z=0.5$  as an example of the relation satellites that accreted at that time would follow if there were no evolution after accretion in the Y12 model.

obvious additional trend is that the RV model predicts that sub-haloes ( $z_{\text{acc}} > 0$ ) host more massive galaxies than host-haloes of equivalent  $M_{\text{peak}}$ . This is precisely the expectation given that sub-haloes generally have larger values of  $V_{\text{peak}}$  than host-haloes as shown in the previous section.

We show the same relations for the M13, B13, and Y12 models in the lower panels of Fig. 6, but instead of showing it for individual galaxies, we show the mean relation as a function  $z_{\text{acc}}$  for simplicity and ease of interpretation. Broadly, to the degree that there is a difference in the relation for centrals and satellites, each of these models predicts the qualitative opposite trend as the RV model; sub-haloes host *less* massive galaxies than host-haloes of equivalent  $M_{\text{peak}}$  at masses less than  $\sim 10^{12.5} h^{-1} M_{\odot}$ . In the M13 and B13 models, this comes about because the SMHM relation for satellites as a function of  $z_{\text{acc}}$  is a fossil record of the relation for centrals at higher redshift since it is assumed that satellites cease to grow appreciably after they are accreted.

On the other hand, the Y12 model predicts almost no difference in the stellar mass between satellites and centrals at fixed halo mass. This is because in the Y12 model satellites are allowed to grow (or lose stellar mass) after accretion. We show the relation at  $z = 0.5$  and  $1.0$  for *centrals* as a dotted line in the Y12 panels in Fig. 6. It is very interesting that the parameter constraints found by Y12 indicate that this happens post accretion evolution happens very efficiently, with satellites achieving a final stellar mass  $> 90\%$  that of centrals at  $z = 0$ . This phenomenology also explains why Y12 predicts a slightly larger satellite fraction than the M13 and B13 models. The sub-halo fraction increases as  $M_{\text{peak}}$  decreases (see Fig. 10), resulting in more satellites as lower  $M_{\text{peak}}$  sub-haloes are populated. The same is true for the RM model compared to the M13 and B13 models. However, this effect in the Y12 and RM models alleviates the clustering decrement only slightly relative to the M13 and B13 models. In the absence of post-accretion evolution of satellites in Y12(c parameter set to 0), the model looks similar to M13 and B13, where satellites are less massive than centrals at  $z=0.0$ . However, it is telling that Y12 strongly prefers large values for  $c$  in the analysis performed in Yang et al. (2012).

#### 4.4 Galaxy Growth Histories

Given that the RV and mass-based models make different assumptions for the SMHM relation, especially regarding satellites, it is not surprising that each model predicts different galaxy clustering signals and satellite abundances. Considering the RV model's success in fitting clustering observations and the mass-based models failure (see §3), it appears that the RV model should be favoured as the more physical. However, in this section we show that the RV model implies galaxy growth histories that are incompatible with both the other models and observations.

In the previous section we showed that, in the RV model, the stellar masses of satellites are on average larger than centrals at fixed  $M_{\text{peak}}$ . This finding implies that the SMHM relation in the RV model decreases over time (evolves towards the right in Fig. 6), while it increases in the other models (evolves from right to left). This conclusion rests on two implicit assumptions of the RV model: the stellar mass of satellites does not evolve significantly after  $z_{\text{acc}}$ , and the

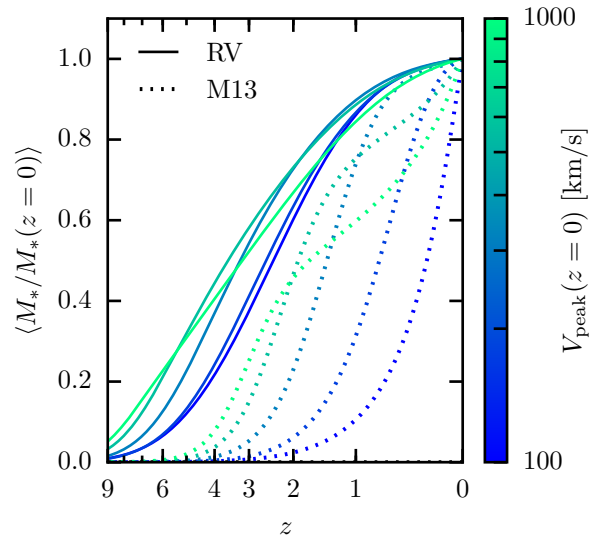


**Figure 7.** The average stellar mass as a function of redshift divided by the mass at  $z=0$  for haloes of various values of  $V_{\text{peak}}$  at  $z=0$  (coloured lines). The prediction from the non-evolving RV model is shown as solid lines. The prediction of the evolving M13 model is shown as dotted lines.  $V_{\text{peak}}(z=0)$  was converted  $M_{\text{vir}}$  using a fitting function in order to directly compare the RV and M13 models. The implied average stellar mass growth histories of haloes are drastically different between the two models. The RV model predicts much earlier stellar mass growth relative to the M13 model.

$M_{*} - V_{\text{peak}}$  (SMVP) relation itself does not evolve. A non-evolving SMVP implies that galaxies grow along the SMVP, i.e. galaxy growth is tied to the growth of  $V_{\text{peak}}$ . In this section we examine the latter assumption, and we leave an examination of post-accretion satellite evolution to §6.

In order to extrapolate the SMVP relation in the RV model to less massive haloes, we fit it with a function of the form:

$$\langle M_{*} | V_{\text{peak}} \rangle = 2M_0 \left( \frac{V_{\text{peak}}}{V_0} \right) \left[ \left( \frac{V_{\text{peak}}}{V_0} \right)^{\alpha} + \left( \frac{V_{\text{peak}}}{V_0} \right)^{\beta} \right]^{-1} \quad (30)$$

We perform a non-linear least squares fit to the median stellar mass in 0.025 dex  $V_{\text{peak}}$  bins. We find the parameters  $\log(M_0/h^{-2} M_{\odot}) = 10.0 \pm 0.01$ ,  $\log(V_0/\text{km/s}) = 2.197 \pm 0.004$ ,  $\alpha = -4.6 \pm 0.1$ , and  $\beta = -0.20 \pm 0.01$  provide an excellent fit. We perform a similar fit to the SMHM relation in the RM model, assuming it does not evolve.

In addition to the form of the SMVP relation, the average growth history of galaxies in RV is dependent on the potential well growth history (PWGH) of haloes,  $\langle V_{\text{peak}} | V_{\text{peak}}(z=0) \rangle(z)$ . Using the PWGHs from van den Bosch et al. (2014), in Fig. 7 we show the implied growth history of galaxies in the RV model for host-haloes with different  $V_{\text{peak}}$  at  $z=0$ . For comparison, we also show stellar mass growth histories from M13, which instead depend on the average mass accretion histories (MAHs) of haloes and

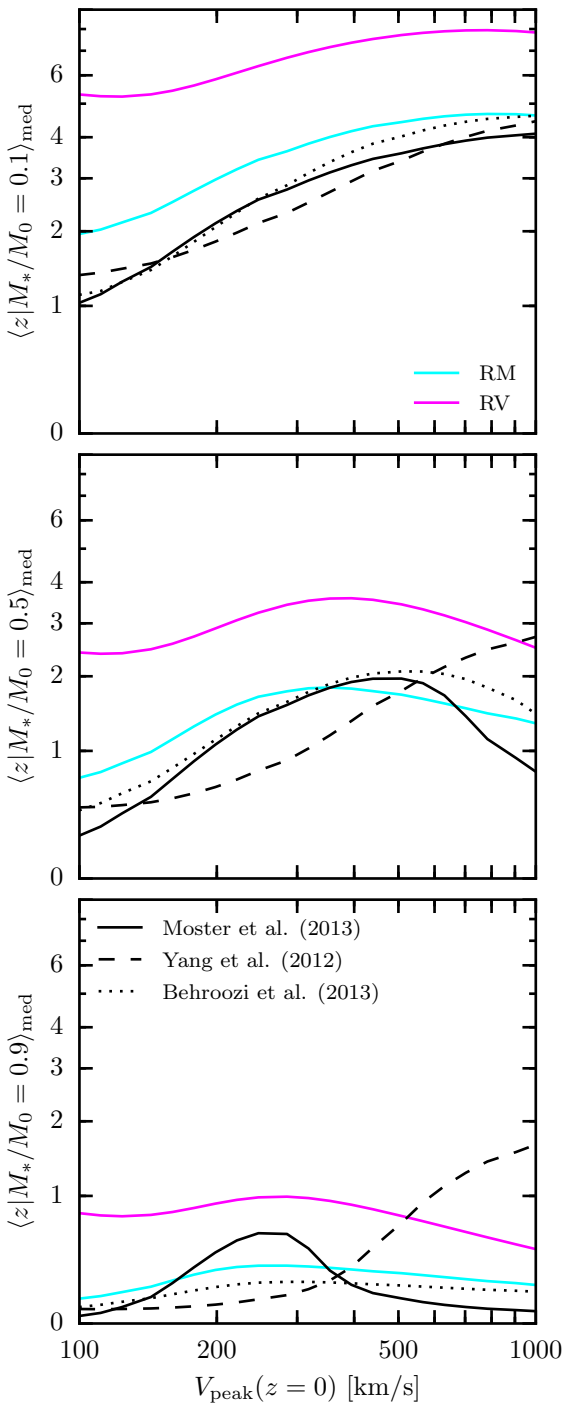


**Figure 8.** The median redshift at which a central galaxy reaches a fraction,  $f$ , of its  $z = 0$  stellar mass as a function  $V_{\text{peak}}$  at  $z = 0$ . The three panels are for  $f = 0.9, 0.5$ , and  $0.1$  from top to bottom, respectively. The lines are for the RM (cyan), RV (solid magenta), M13 (solid black), Y12 (dashed), and B13 (dotted). The RV model consistently forms a larger fraction of galaxies' mass at higher redshift relative to the mass-based models. The only exception to this rule is the Y12 model, where massive galaxies loose mass at low redshift.

the explicitly parametrized evolution of the SMHM relation. Note that we have converted  $M_{\text{peak}}(z = 0)$  to  $V_{\text{peak}}(z = 0)$  using eq. 29 to place these histories on the same figure.

Fig. 7 shows that, in the RV model, galaxy growth is largely self-similar—at any given redshift, galaxies of every mass are growing at similar rates. Conversely, in the M13 model, galaxy growth is much more dependent on halo mass—high mass galaxies form early, growing slowly at low redshift, while low mass galaxies form late. Slow late time growth of massive galaxies is necessary to reproduce the observed prevalence of quiescent galaxies as mass increases (e.g. Wetzel et al. 2012). It is the same story when comparing RV to any of the other mass based models. In Fig. 8, we show the the median redshift galaxies found it different mass haloes at  $z = 0$  reach a fraction,  $f$ , of their  $z = 0$  stellar mass. Mass-based SHAM models generically predict much later growth compared to RV. The one exception to this rule is the Y12 model, where at late times, massive galaxies lose stellar mass. As a result, galaxies found in massive haloes reached 90% of their  $z = 0$  mass relatively early. Since we are not concerned with the evolution of massive galaxies, we do not investigate this aspect of Y12 any further in this paper. Interestingly, even the RM model, where the SMHM relation does not evolve, results in galaxy growth much closer to the evolving models than with RV. This is a consequence of the fact that haloes form their potential wells early, primarily adding mass in the outskirts at late times (van den Bosch et al. 2014). As a result, any model for galaxy formation based on  $V_{\text{peak}}$  will have to decouple galaxy growth from the growth of  $V_{\text{peak}}$  more than models based on  $M_{\text{peak}}$ .

Finally, the effect of the dramatically different growth history in the RV model can be seen in the evolution of the stellar mass function. In Fig. 9 we show the predicted stellar mass function,  $\phi(M_*, z)$ , in the RV model and M13 (which was tuned to reproduce  $\phi(M_*, z)$ ). Here it is clear that the RV model over-produces galaxies, especially below the knee in the mass function.

#### 4.5 $V_{\text{peak}}$ or $M_{\text{peak}}$ ?

Given that the M13, Y12, and B13 models were fit to the stellar mass function at various redshifts and reproduce the cosmic star-formation density in the Universe (among other observables), it is difficult to imagine how to make a model like RV consistent with these same observational constraints. While not explored here, it is likely that a more complicated  $V_{\text{peak}}$  based SHAM model could produce realistic galaxy growth histories, but this would require evolution in the SMVP relation. Any evolution will require the SMVP relation be lower at high redshifts (as is the case for the SMHM relation in M13, Y12, and B13), reducing the stellar mass assigned to satellite galaxies in typical implementations. This sort of modification would result in a decrease in the galaxy clustering signal on small scales.

Given this, it is not clear that there is a reason to prefer a  $V_{\text{peak}}$  based SHAM model over one based on  $M_{\text{peak}}$ . Apart from arguments related to fitting  $w_p(r_p)$  and  $\phi(M_*, z)$ , there are other difficulties that must be overcome if  $V_{\text{peak}}$  is to be argued as more fundamental driving the stellar mass mapping into haloes. For any given (sub)-halo,  $V_{\text{peak}}$  is generally set during major mergers (1:5 or larger, Behroozi et al. 2014a), and if stellar mass is tightly correlated with  $V_{\text{peak}}$ ,

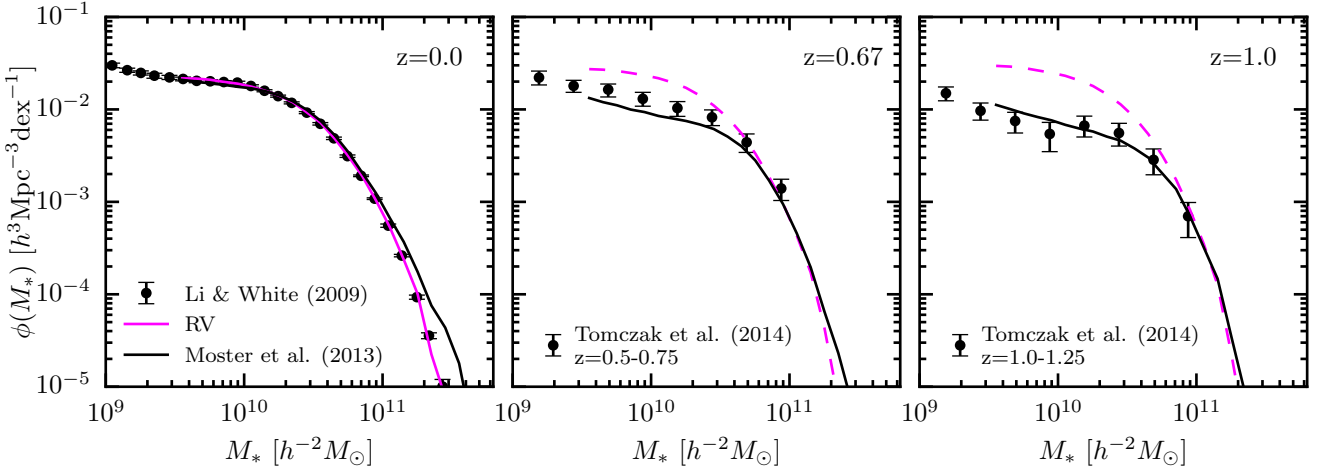


**Figure 9.** The evolution of the stellar mass function is shown for the M13 model (black lines) as well as the implied evolution of the RV model (magenta lines). For comparison, we show observational measurements of the stellar mass function from Li & White (2009) ( $z=0$ ), and Tomczak et al. (2014) ( $z>0$ ).

this would imply bursty star-formation closely tied to major mergers which is not favoured by observations (e.g. star formation histories ?). On the other-hand,  $M_{\text{peak}}$  remains a theoretically attractive as a quantity that should be tightly coupled to stellar mass. Peak halo mass is a good indicator of the amount of baryons that have been available to a galaxy to grow over its history [citations needed].

In our comparison between  $V_{\text{peak}}$ -based SHAM and  $V_{\text{peak}}$ -based SHAM it is clear that there is a tension between fitting galaxy clustering on small scales while simultaneously reproducing the build up of stellar mass in the Universe. This tension presents a “clustering crisis” for SHAM. Our exploration in the preceding sections has suggests multiple avenues SHAM models could be altered in order to alleviate this crisis. We have fingered too few satellites as the culprit for the clustering deficiency in mass based SHAM models. One solution is to simply increase the number of satellites in the mass-based models as many models have found to be necessary. In §5, we examine the plausibility of missing sub-haloes, and thus satellites, in our implementation of the mass-based SHAM models. A significant population of missing sub-haloes would be an indication that so called “orphan” galaxies play an important role in solving the clustering crisis. Apart from orphans, we also consider two other physically motivated modifications to increase the satellite fraction–post-accretion satellite growth in §6 and assembly bias effects in §7.

contrast is low (Wetzel & White 2010; Muldrew et al. 2011; Knebe et al. 2011; Onions et al. 2012; Knebe et al. 2013; van den Bosch & Jiang 2016) as is the case in the central regions of host haloes. If this is in fact occurring, then it is appropriate to include a population of “orphan” galaxies, galaxies that have no identifiable sub-halo within a simulation but should rightfully be included if the simulation or sub-halo finder had been more successful.

After sub-haloes are accreted onto a more massive host halo, mass is tidally stripped as the sub-halo orbits within the potential of its host, resulting in a ratio between the  $z=0$  mass and the mass at accretion that is generally less than unity:

$$f_m = m_{\text{sub}}/m_{\text{acc}} \quad (31)$$

where the mass of a sub-halo,  $m_{\text{sub}}$ , is the instantaneous mass that is bound to the sub-halo, and  $m_{\text{acc}}$  is the viral mass at the time of accretion. Eventually, sub-haloes may simply be stripped below the mass resolution of the simulation,  $f_m \times m_{\text{acc}} \sim m_p$ . If it is common for sub-haloes to survive to this point, this will result in a need for orphans. Alternatively, if sub-haloes are not tracked accurately, mass resolution is not sufficiently high, or the force resolution is not sufficient, some sub-haloes may become disrupted prematurely, meaning fewer sub-haloes will be available to host satellite galaxies when applying an abundance matching scheme.

Here we estimate the contribution of this potential missing sub-structure to the abundance of sub-haloes. In the upper panel of Fig. 10, we measure the sub-halo fraction as a function of  $M_{\text{peak}}$  at  $z=0$  in 0.2 dex mass bins:

$$f_{\text{sub}} = \frac{N_{\text{sub}}}{N_{\text{sub}} + N_{\text{host}}} \quad (32)$$

Jiang & van den Bosch (2016) and van den Bosch & Jiang (2016) show that the evolved conditional sub-halo mass function is well approximated by a power law with a universal low mass end slope. Given this, it is expected that  $f_{\text{sub}}$  will

## 5 ORPHAN GALAXIES

One possible solution to the lack of small scale clustering signal in SHAM models is to include a population of “orphan” galaxies. Given the finite mass resolution of dark matter simulations, it is reasonable to expect that some sub-haloes are artificially disrupted or otherwise missing from the halo catalogues at  $z=0$  (Guo & White 2013). Alternatively, sub-halo finders may fail in identifying sub-haloes when the density

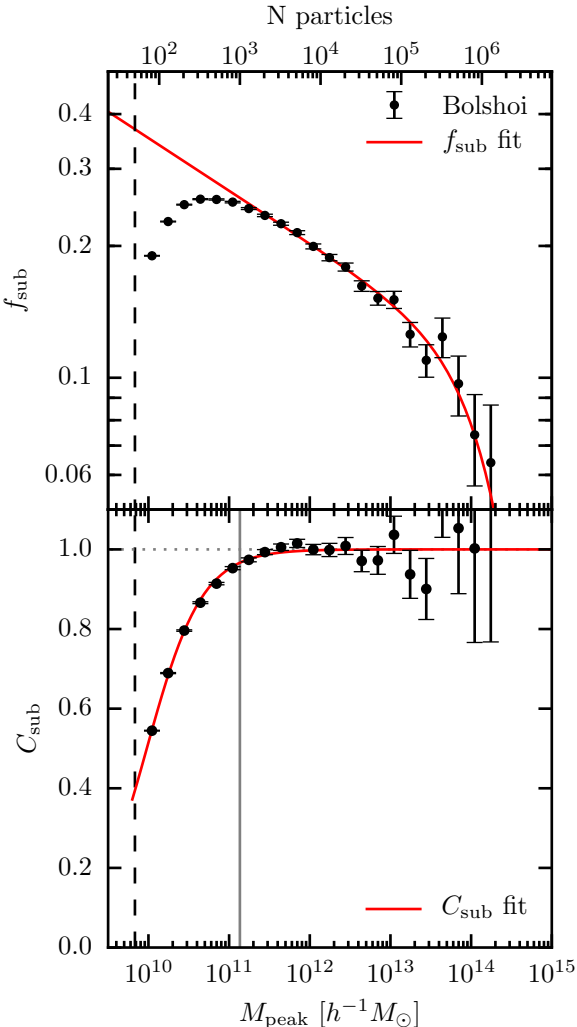


**Figure 10.** The upper panel shows the fraction of haloes that are sub-haloes,  $f_{\text{sub}}$ , as a function of  $M_{\text{peak}}$  in the Bolshoi simulation (points with error bars). This relation is fit with a Schechter function (eq. 33, red line) down to  $10^{12} h^{-1} M_{\odot}$  and extrapolated to lower masses. The lower panel shows an estimate of the sub-halo completeness,  $C_{\text{sub}}$ . This relation is fit with a function (eq. 34, red line). The dashed line marks the 50 particle  $M_{\text{peak}}$  minimum mass a (sub-)halo must attain to be included in our halo catalogue. The grey line indicates the 1000 particle mass limit Guo & White (2013) recommend for convergence in sub-halo abundance. The upper x-axis is the number of particles corresponding to  $M_{\text{peak}}$  on the lower axis. The error bars indicate Poisson Errors.

be a monotonic power law, increasing towards lower halo masses.

With this in mind, we fit  $f_{\text{sub}}$  in Bolshoi with a Schechter function of the form:

$$f_{\text{sub}}(M_{\text{peak}}) = f_0 \left( \frac{M_{\text{peak}}}{M_0} \right)^{\alpha} e^{-M_{\text{peak}}/M_0} \quad (33)$$

We find a good fit with  $f_0 = 0.105 \pm 0.006$ ,  $\log(M_0/h^{-1} M_{\odot}) = 13.4 \pm 0.1$ , and  $\alpha = -0.120 \pm 0.005$  as shown as the red line in the upper panel of Fig. 10.

There is a prominent break in the the sub-halo fraction at  $\sim 10^{11} h^{-1} M_{\odot}$ , approximately 1.5 dex above the halo mass identification limit imposed on the simulation,  $50 \times m_p$ . Therefore, we conservatively use only the measurements above  $10^{12} h^{-1} M_{\odot}$  for our fit to  $f_{\text{sub}}$ .

We calculate the sub-halo completeness in the simulation as the ratio of the empirical  $f_{\text{sub}}$  and the fit using eq. 33 as shwon in the bottom panel of Fig. 10. We then model the completeness,  $C_{\text{sub}}$ , as a function of halo mass as:

$$C_{\text{sub}}(M_{\text{peak}}) = \frac{C_0}{1.0 + \left( \frac{M_0}{M_{\text{peak}}} \right)^{\gamma}} \quad (34)$$

We find  $\log(M_0/h^{-1} M_{\odot}) = 9.980 \pm 0.003$  and  $\gamma = 1.27 \pm 0.02$  provide a good fit, as shown by the red line in the bottom panel in Fig. 10. For now, we fix  $C_0 = 1.0$ , and we examine the possibility of  $C_0 < 1.0$  at the end of this section. The implicit assumption here is that when sub-haloes are well resolved, as is the case for massive (sub-haloes) at the time of infall, there should be no missing sub-structure. Our estimation of the completeness is broadly consistent with the 1000 particle threshold found by Guo & White (2013) using the Millennium simulation suite. Furthermore, we find that  $C_{\text{sub}}(M_{\text{peak}})$  is very nearly constant with redshift ( $z = 0-4$ ).

The SHAM models considered in this work require sub-haloes in order to populate the simulation with satellites. To create sub-haloes to host orphan galaxies we “clone” extant sub-haloes in the regime where incompleteness results in too few sub-haloes. Here we briefly describe this process and leave a detailed description to Appendix C. Where needed, we create a copy of a sub-halo (hereafter ‘clone’) and place it into a new host-halo with approximately the same mass as the donor’s host-halo. We consider two methods for assigning positions and velocities to these new clone sub-haloes that host orphans. One method conserves the relative position and velocity with respect to the donor’s host-halo (**sub-profile**). The other method assigns the clone the position and velocity of a randomly selected particle in its new host-halo (**dm-profile**). We carry over all other relevant properties from donor to clone. We then add clones into the simulation to make up for incompleteness.

We find that when populating the Bolshoi simulation down to  $M_* \geq 10^{9.5} h^{-2} M_{\odot}$  using our model for  $C_{\text{sub}}$ , less than  $\sim 1\%$  of satellite galaxies are orphans in each of the SHAM models. This small orphan percentage suggests that the Bolshoi simulation has sufficient resolution for SHAM studies down to the stellar masses considered in this paper. Of course, populating these models down to lower masses would result in a larger contribution from orphans. Nevertheless, we examine the effect of this small orphan population on the galaxy clustering predictions of each SHAM. We find that the maximum effect on  $w_p$  is of order  $\sim 1\%$  on the clustering signal at  $0.1 h^{-1} \text{Mpc}$ , regardless of the method used to assign orphan positions in their host. As expected, the effect of these orphans is even smaller in the more massive stellar mass bins were the  $C_{\text{sub}}$  correction is smaller. We conclude that the resolution of the Bolshoi simulation appears to be sufficient for SHAM studies down to the stellar masses considered here and most relevant for galaxy clustering studies using SDSS.

Finally, we ask “how many orphans are needed to increase the clustering signal sufficiently in the SHAM models

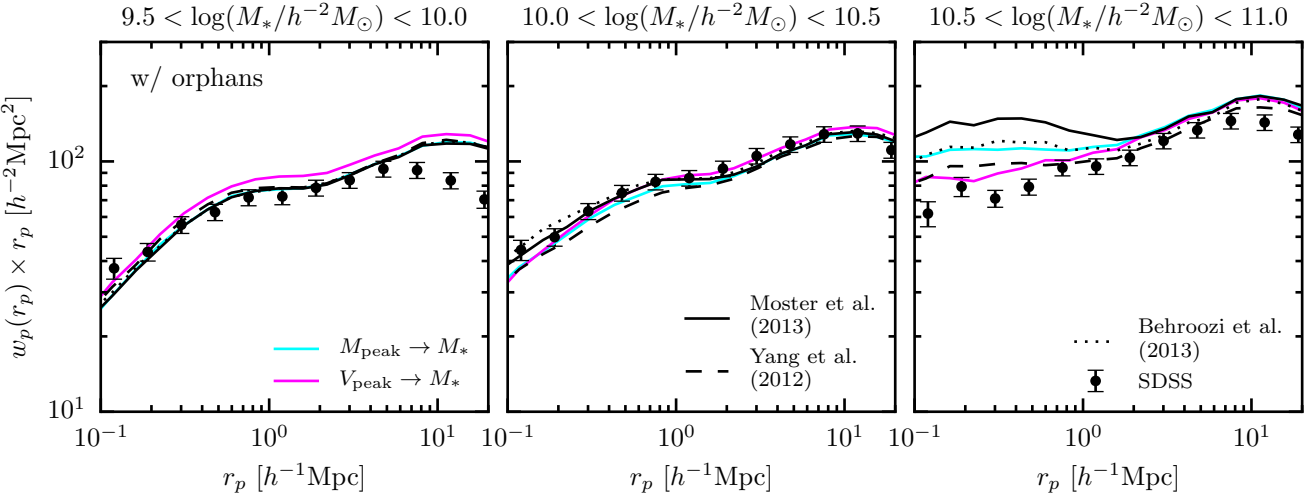


**Figure 11.** The projected correlation function,  $w_p$ , is plotted in three stellar mass bins for five SHAM models (lines) where we have introduced orphan galaxies into each model in order to approximately match the clustering in the  $[10.0, 10.5]$  log stellar mass bin. For comparison, we plot the projected correlation function of galaxies in SDSS as measured by Yang et al. (2012) as points with error bars. Compare this to figure 3 for the case with no orphans.

774 based on  $M_{\text{peak}}$ ?" To answer this question, we adjust  $C_0$  in  
 775 eq. (34), while keeping the other parameters fixed, and fit to  
 776 the galaxy clustering observations. Lower values of  $C_0$  imply  
 777 an overall increased population of clone sub-haloes available  
 778 to host orphans at all masses. This correction assumes that  
 779 sub-haloes are being artificially disrupted or merged with  
 780 the host *at all masses*. For each model,  $C_0$  was adjusted in  
 781 order to best fit the galaxy clustering signal in the inter-  
 782 mediate mass bin ( $10.0 \leq \log(M_*/h^{-2}M_\odot) < 10.5$ ). The  
 783 result of this exercise is shown in Fig. 11 using the sub-  
 784 profile method to assign the positions and velocities. We  
 785 find that each model requires  $C_0 = [0.6, 1.0, 0.4, 0.5, 0.5]$ ,  
 786 for the RM, RV, M13, Y12, and B13 models respectively.  
 787 While the RV model does not require orphans, the mass-  
 788 based SHAM models require that on average approximately  
 789 *half of all satellites are orphans*. In Fig. 12 we show how  
 790 assigning orphans positions within their host affect the cluster-  
 791 ing predictions for the M13 model in the intermediate mass  
 792 bin only. As expected, using dm-profile boosts the clustering  
 793 signal at small scales relative to sub-profile, but the effect  
 794 is small compared to the dependence on  $C_0$ . This trend is  
 795 largely similar at the other mass considered and for the other  
 796 SHAM models.

797 We make no attempt to fit for new parameters in the  
 798 evolving SMHM models using our orphan model and clus-  
 799 tering measurements, while the RM and RV models adjust  
 800 automatically to the increased abundance of sub-haloes. Ad-  
 801 justing the population of sub-haloes so drastically in the  
 802 evolving models will have an effect on the parameter in-  
 803 ference for the SMHM relation. With this caveat in mind,  
 804 the most noticeable failure of the mass-based models is  
 805 the over-prediction of the small scale ( $< 1\text{Mpc}$ ) cluster-  
 806 ing signal in the most massive stellar mass bin ( $10.5 \leq$   
 807  $\log(M_*/h^{-2}M_\odot) < 11.0$ ). Each of these models now produce  
 808 too many massive satellites. This problem could be reduced  
 809 by altering the SMHM for massive satellites or reducing the

810 number of massive orphans. We leave a detailed study on  
 811 the self-consistently including orphan galaxies in SHAM to  
 812 future work.

813 The Y12 model model when fit to galaxy clustering in  
 814 Yang et al. (2012), which used an analytic halo model and  
 815 let the sub-halo abundance be a free parameter, finds results  
 816 which are consistent with our finding here that  $C_0 \sim 0.5$ ,  
 817 namely that the sub-halo abundance needs to be approx-  
 818 imately a factor of two larger than that in Bolshoi. Fur-  
 819 thermore, Jiang & van den Bosch (2016) find that the un-  
 820 evolved (peak sub-halo mass) surviving (not disrupted) sub-  
 821 halo mass function is approximately a factor of two lower  
 822 than the unevolved sub-halo mas function. This suggest a  
 823 plausible source of the missing sub-haloes needed to host  
 824 orphans could be artificially disrupted sub-haloes.

## 825 6 SATELLITE GROWTH

826 While we have shown that a large population of "orphan"  
 827 galaxies would alleviate the clustering crisis in mass-based  
 828 SHAM models, high resolution dark matter simulations do  
 829 not seem to provide evidence of the requisite missing sub-  
 830 halo population. With this in mind, we explore alternative  
 831 mechanisms to boost the galaxy clustering signal in SHAM  
 832 models. In this section, we consider whether continued star-  
 833 formation in satellites after accretion can significantly boost  
 834 clustering. This is motivated by findings that suggest satel-  
 835 lites continue to form stars and grow in stellar mass after  
 836 accretion for between  $\sim 2$  and  $4$  Gyr (Wetzel et al. 2013).  
 837 If satellites continue to grow after accretion, SHAM meth-  
 838 ods which use the SMHM relation at the time of accretion  
 839 to assign stellar mass to satellites will under-estimate their  
 840 stellar mass (e.g. M13 and B13).

841 It is a common assumption of SHAM models, implicit  
 842 or explicit, that satellites undergo no significant evolution in  
 843 stellar mass after the time of accretion. Amongst the mod-

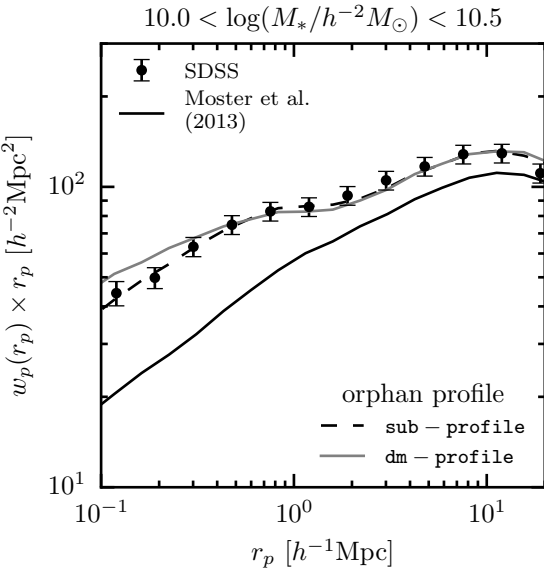


**Figure 12.** Comparison of the effect of the profile orphan galaxies follow in their host-halo on galaxy clustering. The solid line shows the clustering prediction for the original M13 model. The dashed line is M13 including orphans which follow the same profile as extant sub-haloes in the simulation with  $C_0 = 0.4$ . The grey line is the same model where orphans are more centrally concentrated, following the profile of dark matter in their host. See Appendix C for a more detailed discussion. For comparison, SDSS measurements by Yang et al. (2012) are plotted as points with error bars.

els considered in this work, the Y12 model serves as the exception, explicitly parametrizing post-accretion evolution. In that model, satellites are assigned a stellar mass at  $z=0$  that is between the one achieved at the time of accretion and the one a central galaxy with the same peak halo mass at  $z=0$  achieves. The growth (or mass loss) is controlled by the “c” parameter in eq. (22) as explained in §2.1.4. In the case where  $c=1$ , satellites follow the same SMHM as centrals at  $z=0$  regardless of the time of accretion. For  $c=0$ , the model is similar to B13 and M13, with no evolution in the mass of satellites occurring after accretion. For this work, we set  $c = 1$  (consistent with SMF2 FIT-2PCF in table 4 in Yang et al. 2012). The result is a model similar to the RM model, where no distinction is made between central galaxies and satellites when abundance matching on  $M_{\text{peak}}$  at  $z=0.0$ . While such a model does produce more massive satellites than the M13 and B13 models, the RM and Y12 models still result in a clustering signal that is too weak.

In order to further explore the effect of satellite growth, we devise a different model for post accretion evolution similar to that implemented in Behroozi et al. (2015). Our primary assumption is that satellites form stars *exactly* like central galaxies which occupy haloes that had the same mass as the satellite’s halo at the time of accretion,  $t_{\text{acc}}(z_{\text{acc}})$ , before quenching rapidly after a delay time,  $\Delta t_q$ . Within the SHAM framework, stellar mass is assigned to (sub-)haloes using a mass proxy,  $\mathcal{M}$ . To implement our growth model, we set  $\mathcal{M}$  for sub-haloes to the average mass of a host-halo

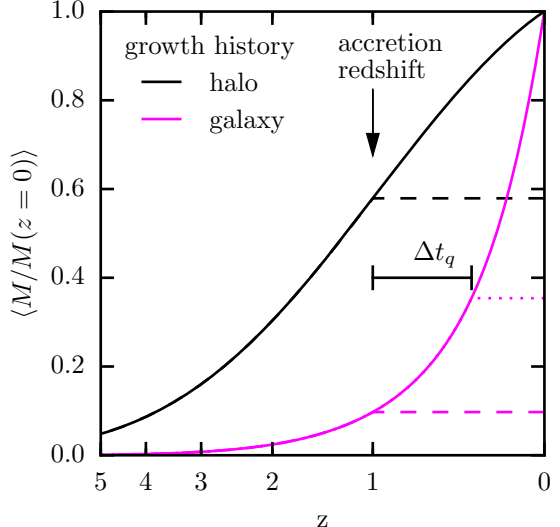


**Figure 13.** As an example, the average growth history of a halo (black solid line) with a  $z=1$  mass of  $10^{11} h^{-1} M_\odot$  that remains a distinct halo to  $z=0$  and the average stellar mass of a galaxy which occupies such a halo (magenta solid line) in the M13 model are plotted. The growth histories are normalized by the  $z=0$  mass. Additionally, the average peak halo mass for a sub-halo which is accreted onto a host-halo at  $z=1$  and survives till  $z=0$ , is plotted as a dashed black line (here peak mass is assumed to be set at the time of accretion). Two different satellite growth models are shown. A model where the mass of the satellite is set at the time of accretion and no further growth occurs is shown as a dashed magenta line—no further growth occurs after accretion. A model where a satellite continues to grow for some time,  $\Delta t_q = 4$  Gyr, after accretion, just as a central which occupies a halo of equal mass to the sub-halo at the time of accretion, is shown as a dotted line. A significant amount of stellar mass can be acquired after accretion in such a model.

at  $t_{\text{acc}} + \Delta t_q$  which had the same mass as the sub-halo at  $t_{\text{acc}}$ :

$$\mathcal{M} = \langle M_{\text{vir}}(t_{\text{acc}} + \Delta t_q) | M_{\text{vir}}(t_{\text{acc}}) = M_{\text{acc}} \rangle \quad (35)$$

To extrapolate the mass from  $t_{\text{acc}}$  to  $t_{\text{acc}} + \Delta t_q$  we use the average MAHs of haloes (van den Bosch et al. 2014).

In Fig. 13 we describe the components of this model. Consider two galaxies, one destined to be a central galaxy at  $z=0$ , and another that becomes a satellite at  $z=1$ . Each reside in a halo with mass  $10^{11} h^{-1} M_\odot$  at  $z=1$ . We show  $\mathcal{M}(z)$  for such a halo and sub-halo as a black solid and dashed line normalized by the  $z=0$  mass of the host-halo. The average stellar mass growth history for the central galaxy in the host halo (from the M13 model) is shown as a solid magenta line normalized by the  $z=0$  stellar mass. The growth history of the satellite galaxy is shown as a long dashed magenta line. In a model where no evolution occurs post accretion, the stellar mass of the satellite is set by the stellar mass at accretion. Our post-accretion growth model is shown as a dotted line—the satellite continues to grow for  $\Delta t_q = 4.0 h^{-1} \text{Gyr}$  after accretion just as it would have if it remained a central galaxy. In this specific example the satellite’s stellar mass

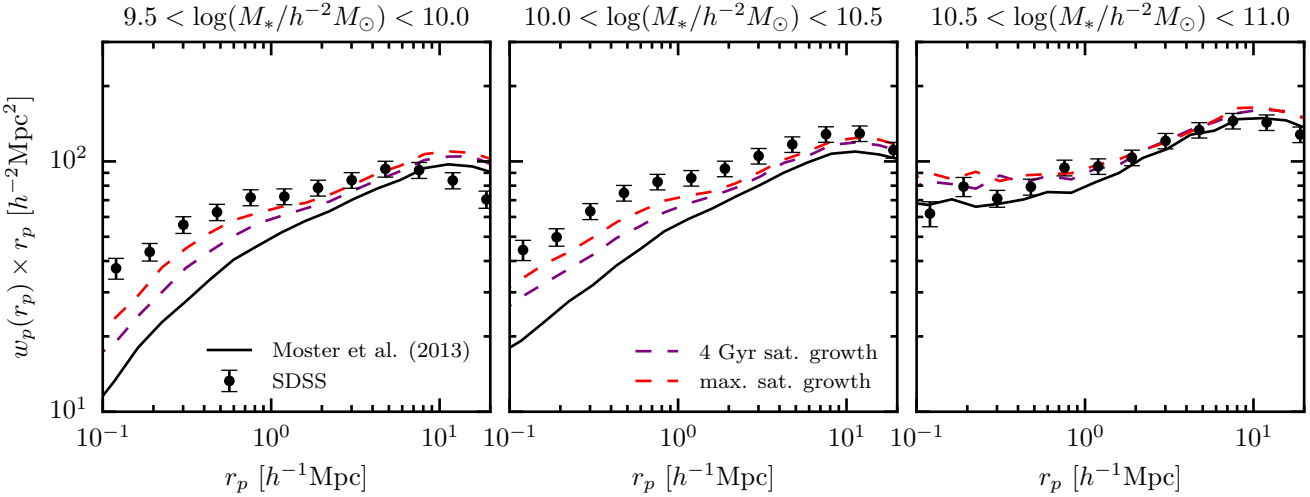


**Figure 14.** Similar to figure 3. The original M13 model is shown as a solid line. The effect of allowing satellites to grow as described in §6 for 4 Gyr (purple dashed line) and till  $z=0.0$  (purple dashed line).

increases by 350% compared to M13 with no post-accretion growth. In general, the amount a satellite will grow in a fixed  $\Delta t_q$  will depend on the accretion time and the peak halo mass. Recently accreted sub-haloes will have less time to grow, and massive sub-haloes will only grow slightly as massive galaxies do not grow rapidly at late times.

We apply this model for satellite growth to the M13 and B13 models. Initially, we set  $\Delta t_q = 4 h^{-1}$  Gyr. We show the result on the clustering for the M13 model in Fig. 14 as an example (purple dashed line). In each model,  $\Delta t_q = 4 h^{-1}$  Gyr does not result in a sufficient increase in the clustering signal. To estimate an upper bound on the effect of such a satellite growth model, we allow satellites to grow till  $z=0$ . This result is shown in Fig. 14 as a red dashed red line. Interestingly, even this extreme satellite growth model does not result in strong enough galaxy clustering relative to the observations. The results for the B13 model are very similar.

The failure of our growth model to fit galaxy clustering observations suggest that satellite growth (at least as implemented here) cannot on its own solve the clustering crisis; however, reasonable growth does have a significant effect on the clustering signal at small scales. This also suggests that the growth model used by Y12 is not sufficient to capture post-accretion growth. In Y12, a satellite is limited to grow only as massive as a central at  $z=0$  with the same peak mass. In the growth model considered here, satellites may grow more massive than centrals by  $z=0.0$ . Any SHAM model that aims to fit galaxy clustering should take such an effect into account.

## 7 GALAXY ASSEMBLY BIAS

Assembly bias is a phenomenon observed in  $\Lambda$ CDM simulations of structure formation that the clustering of haloes is affected by formation history in addition to mass (Gao et al. 2005; Wechsler et al. 2006; Gao & White 2007; Li et al. 2008; Sunayama et al. 2015). However, the degree to which the properties of galaxies themselves are influenced

by the assembly history of their halo remains an open question. SHAM algorithms that employ measures of  $V_{\max}$  (like the RV model) already induce assembly bias into galaxies because concentration, and therefore circular velocity, is correlated with formation history at fixed halo mass (Zentner et al. 2014). Conditional abundance matching (CAM, Hearin et al. 2014) extends the SHAM framework by allowing for two or more halo properties to influence how galaxy properties are assigned in the SHAM algorithm. CAM has been used to study the dependence of star-formation rate and halo formation history (Hearin & Watson 2013; Hearin et al. 2014; Watson et al. 2015; Saito et al. 2015; Paranjape et al. 2015); however, SHAM models that assign stellar mass and star-formation in a self-consistent manner are still in development.

In this section we examine whether introducing assembly bias into the galaxy-halo mapping can increase the satellite fraction and galaxy clustering signal in mass-based SHAM models. Specifically, we consider a model where  $M_*$  is correlated with the formation history of the (sub-)halo it occupies such that early forming haloes host more massive galaxies than late forming haloes at *fixed* peak (sub-)halo mass. While many measures of halo formation history have been employed, for this work we use the redshift a halo first achieves a fraction,  $f$ , of its peak halo mass,  $z_f$  (see Appendix A for details on how  $z_f$  is calculated).

### 7.1 Rank Order SHAM Assembly Bias

We begin by inducing assembly bias in the RM model. In order for assembly bias to have any effect on  $M_*$ , there must be a significant amount of scatter in the SMHM relation,  $\sigma_{\log(M_*)} > 0$ . Scatter provides a dynamic range in  $M_*$  at fixed  $M_{\text{peak}}$  over which  $M_*$  can be correlated with formation history. In Fig. 15 we show some constraints on  $\sigma_{\log(M_*)}$  from the literature. Typical values found for  $\sigma_{\log(M_*)}$  are between 0.1 – 0.2 dex (More et al. 2011; Reddick et al. 2013; Zu & Mandelbaum 2015b; Tinker et al. 2016); however, these

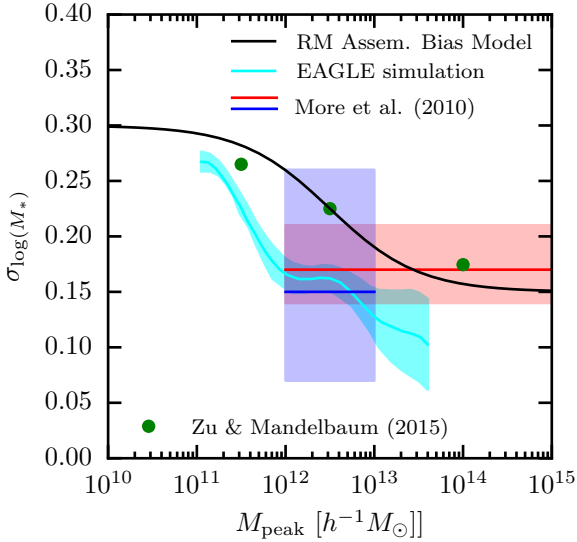


**Figure 15.** Here we plot the log-normal scatter in stellar mass as a function of peak halo mass for our model as a solid black line. For comparison, we show various measurements and theoretical prediction for the scatter. The cyan line and shaded region shows the relation for central galaxies in the EAGLE simulation with the 1-sigma errors (Matthee et al. 2016). The red and blue lines with shaded regions show the fixed scatter determined for red and blue central galaxies and the associated error measured from satellite kinematics (More et al. 2011). The green points show the scatter at three masses determined from an HOD analysis with weak lensing measurements (Zu & Mandelbaum 2015b).

values are most strongly constrained at high masses,  $M_{\text{vir}} > 10^{12} h^{-1} M_{\odot}$ . We add scatter to the SMHM in the RM model as described Appendix ??, parametrizing the level of scatter as a function of halo mass,  $\sigma_{\log(M_*)}(M_{\text{peak}})$ .

To induce a correlation between  $M_*$  and  $z_f$  we bin (sub-)haloes in small 0.1 dex  $M_{\text{peak}}$  bins. We then rank order (sub-)haloes by  $z_f$  and galaxies by  $M_*$ , re-assigning the most massive galaxies to the earliest forming (sub-)haloes in the bin. We use  $f = 0.5$ , the redshift where a (sub-)halo reaches half its peak mass. Furthermore, we parametrize the strength of this correlation by the Spearman’s rank order correlation coefficient,  $\rho(M_{\text{vir}})$ . We weaken the correlation by degrading the rank ordering as described in appendix D in order to reduce the effect of assembly bias on  $M_*$ .

Initially we try a model with fixed scatter,  $\sigma_{\log(M_*)} = 0.18$  dex (similar to the other mass-based models), and a constant maximum ( $\rho = 1$ ) correlation between  $M_*$  and  $z_f$  produces a poor fit to the observed galaxy clustering signal. The fraction of massive galaxies that are satellites in this model is unrealistically large, and the clustering signal increases dramatically at high stellar masses. At the same time, there is relatively little effect on the clustering signal at lower stellar masses. This can be understood as a result of the SMHM relation becoming steep at the low mass end, and  $\sim 0.18$  dex scatter in the SMHM relation is not sufficient to increase the satellite fraction enough.

With this in mind, we modify this simple model to fit

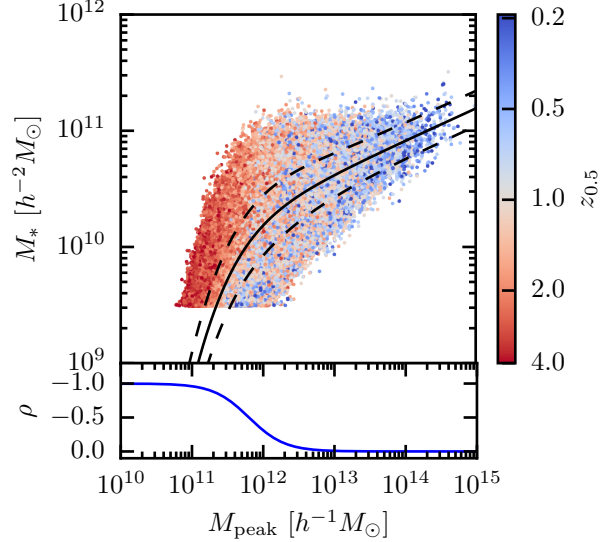


**Figure 16.** In the upper panel, we plot the SMHM relation for individual galaxies as points, colour-coded by the formation redshift,  $z_{0.5}$ . The mean relation is plotted as a solid line with the  $\pm 1\sigma$  scatter shown as dashed lines. In the bottom panel, we show the strength of assembly bias, parametrized by the  $\rho$  parameter.

the observed galaxy clustering signal in two ways. First, we allow the scatter in the SMHM relation to be a function of  $M_{\text{peak}}$ . Specifically, we require the scatter to increase at lower halo masses ( $< 10^{12} h^{-1} M_{\odot}$ ) and decrease at high halo masses ( $> 10^{12} h^{-1} M_{\odot}$ ). While there are few constraints on the scatter in low mass haloes, there are some indications that it may increase as mass decreases. In Fig. 15, we show some observational and theoretical constraints on the scatter.

First, we model the dependence of scatter on halo mass in the modified RM model as:

$$\sigma_{\log(M_*)}(M_{\text{peak}}) = f(M_{\text{peak}}) \quad (36)$$

where  $f$  is a sigmoid function of the form,

$$f(x) = \frac{y_1 - y_0}{1 + e^{k(x - x_0)}} + y_0 \quad (37)$$

By trial and error, we find parameters:  $\log(x_0) = 12.0$ ,  $y_1 = 0.3$ ,  $y_0 = 0.15$ , and  $k = 2.0$  provide good results and are broadly within the scope of values found in other studies (shown as a black line in Fig. 15). The resulting SMHM relation is shown in the top panel of Fig. 16. Second, we require the effect of assembly bias to be minimal at high masses, where there is no need to increase the clustering signal, and stronger at low masses. Similar to the model for scatter, we parametrize the strength of assembly bias,  $\rho$ , as a function of halo mass using the same functional form:

$$\rho(M_{\text{peak}}) = f(M_{\text{peak}}) \quad (38)$$

Through trial and error, we find parameters:  $\log(x_0) = 11.8$ ,  $y_1 = -1.0$ ,  $y_0 = 0.0$ , and  $k = 4.0$  provide good results. In the bottom panel of Fig. 16, we show our model for  $\rho$ .

The clustering signal in this model is shown in Fig. 17

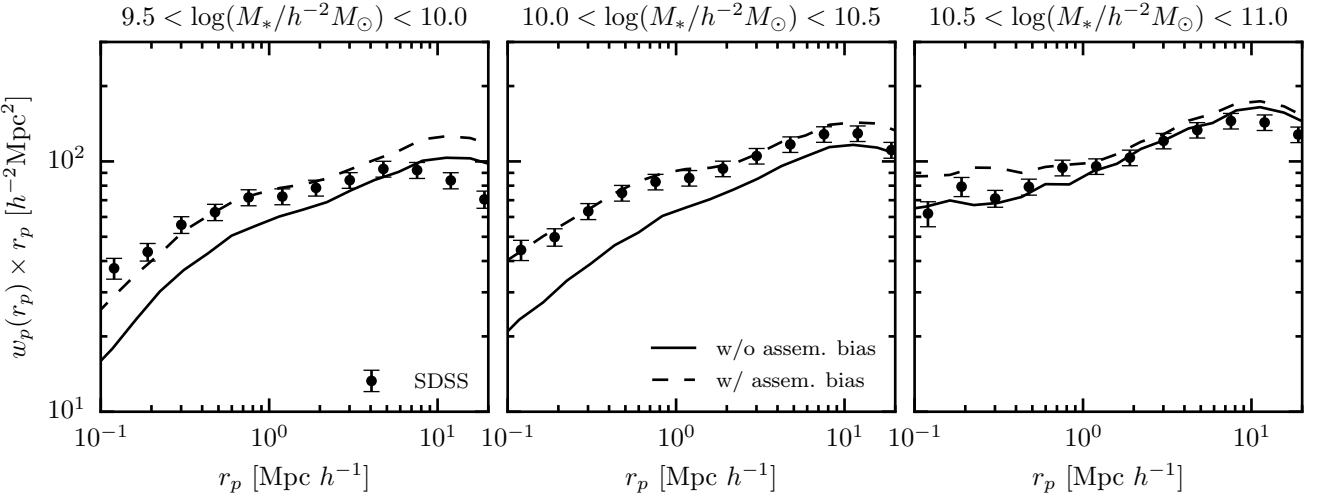


**Figure 17.** Similar to figure 3. The original RM model is shown as a solid line. The combined effect of including assembly bias with scatter in the SMHM relation is shown as a dashed line.

along with the original RM model with no assembly bias. The model with assembly bias is much more consistent with galaxy clustering observations. Furthermore, the satellite fraction is increased to  $\sim 27\%$ , similar to the RV model. This is an indication that assembly bias can increase the satellite fraction and therefore the clustering signal in SHAM models.

However, we find that no formation time parameter is sufficient to increase the stellar mass of satellites enough to affect the clustering signal in each model substantially. The earliest formation time we try in this model is  $z_{0.1}$ , which results in the weakest effect. The most recent we try is  $z_{0.9}$ , which results in the strongest effect. However, even using  $z_{0.9}$  only increases  $f_{\text{sat}}$  in the B13 or M13 models by only  $\sim 2 - 3\%$ , resulting in a minimal effect on galaxy clustering.

## 7.2 Evolving SHAM Assembly Bias

Given the success of our modifications to the RM model to introduce assembly bias to  $M_*$ , we now consider modifications to the evolving mass-based models. As discussed, each of the evolving models makes the assumption that satellite galaxies at the time of accretion have the same mass as central galaxies in haloes with equal  $M_{\text{peak}}$ . In these models, correlating  $M_*$  with  $z_f$  will increase the mass of satellite galaxies if haloes which become sub-haloes form significantly earlier than haloes which remain host haloes. This differs from the model for post-accretion satellite growth discussed in the previous section as satellites will already be more massive than centrals in similar haloes at the time of accretion.

For the evolving models we adopt the same scatter model used for the RM model as described above. Furthermore, for each (sub)-halo, we compare its formation time,  $z_f$ , to the full  $p(z_f | M_{\text{peak}}, z_{\text{acc}})$  of all host-haloes of equivalent mass at the redshift of accretion (for host haloes we set  $z_{\text{acc}} = 0$ ) to find its associated percentile location in the distribution,  $p_f$ . We then assign stellar mass to (sub)-haloes by modifying eq. 25 such that the scatter is now correlated with  $z_f$ :

$$\log[M_*(M_{\text{peak}}, a_{\text{acc}})] = \log[\langle M_* | M_{\text{peak}} \rangle(a_{\text{acc}})] + \mathcal{F}^{-1}(0, \sigma_{\log(M_*)}, 1 - p_f) \quad (39)$$

where  $\mathcal{F}^{-1}(0, \sigma_{\log(M_*)}, 1 - p_f)$  is the quantile function of a normal distribution with mean 0 and log-scatter  $\sigma_{\log(M_*)}$ . In this way, galaxies with earlier formation times are assigned larger stellar masses.

## 8 DISCUSSION & SUMMARY

We have shown that there is no published sub-halo abundance matching (SHAM) model that simultaneously:

- (i) fits the clustering of galaxies at  $z=0$ ,  $w_p(r_p)$ ,
- (ii) reproduces the evolution of the stellar mass function,  $\phi(M_*, z)$ ,
- (iii) and uses only identified, extant, sub-haloes in high resolution dark matter simulations.

Models that fit observations of galaxy clustering are incompatible with the observed evolution of the stellar mass function and expectations for the build up of stellar mass in haloes. Conversely, SHAM models which self-consistently fit the stellar mass function as it evolves significantly under-predict galaxy clustering signals at small scales ( $\leq 1 h^{-1} \text{Mpc}$ ). This tension exposes a clustering “crisis” for SHAM.

Of the five different models examined in this work, only SHAM based on rank ordering (sub-)haloes by peak maximum circular velocity,  $V_{\text{peak}}$ , (RV model) results in a robust galaxy clustering signal consistent with observations. This finding is in-line with previous work that finds  $V_{\text{peak}}$  is the best quantity to consider when fitting galaxy clustering observations (Reddick et al. 2013; Lehmann et al. 2015). However, an implicit assumption in  $V_{\text{peak}}$  SHAM is that the stellar mass- $V_{\text{peak}}$  (SMVP) relation does not evolve. Because haloes grow their potential wells early (e.g. van den Bosch

et al. 2014), a non-evolving SMVP relation results in haloes building up stellar mass too early.

SHAM models based on peak halo mass,  $M_{\text{peak}}$ , (RM, M13, B13, and Y12 models) do not produce strong enough clustering signals with respect to observations, especially on small scales. Evolving models like M13, B13, Y12, and more recently by Rodríguez-Puebla et al. (2017), have been used to learn about the star-formation history of galaxies, quenching physics, and the contribution of merging to the build up of galaxies and stellar haloes with significant success. Given the wide-ranging utility of these models, we have examined three modifications to mass-based SHAM models that alleviate the clustering crisis to varying degrees: the addition of orphan galaxies, stellar mass growth post-accretion for satellites, and assembly bias. Each of these “solutions” addresses the clustering crisis by increasing the number of satellite galaxies.

This tension between fitting clustering observations and abundance of satellites is what drives the demand for increasing the number of satellites in many other studies. For example, in the original semi-analytic implementation of the Y12 model, Yang et al. (2012) find a need for more massive satellites and longer sub-halo survival times than traditional SHAM implementations. It is only when we apply the Y12 model to dark matter simulations directly, that it becomes clear that there are not enough extant sub-haloes to fit clustering observations. Lim et al. (2016) find a similar result when fitting the conditional stellar mass function (CSMF), i.e. satellite abundances. Only models which allow for a significant orphan population can provide a good fit the faint end of the CSMF, another indication that the true culprit in the clustering crisis is a lack of satellite galaxies. Furthermore, this problem is not unique to SHAM models. Pujol et al. (2017), in a comparison of many galaxy formation models, find that only models with orphan galaxies are able to fit clustering observations on small scales.

While the need for orphan galaxies is well established, the motivation for the missing sub-haloes associated with orphan galaxies in high resolution simulations is lacking. While the mass resolution of simulations places an absolute limit on their ability to resolve highly stripped sub-haloes (no structures can exist below the particle mass,  $m_p$ ), we find no empirical evidence of sufficiently massive missing sub-haloes. By examining the power-law behaviour of the sub-halo fraction, we find that the resolution of the Bolshoi simulation,  $m_p = 1.35 \times 10^8 h^{-1} M_\odot$ , appears to be sufficient to model SDSS-like galaxy samples ( $M_* \geq h^{-2} M_\odot$ ), where the majority of satellite galaxies live in haloes with peak masses  $\gtrsim 1000 \times m_p$ . This finding is consistent with an independent analysis based on the convergence of the galaxy clustering signal (Guo & White 2013) from SHAM models. Despite the lack of evidence for large numbers of missing sub-haloes, we find that mass-based SHAM models require that approximately half of all satellite galaxies are orphans in order to fit galaxy clustering observations. This large fraction of orphan galaxies is similar to the number required by Yang et al. (2012).

Regardless, the appeal of SHAM is based on its ability to leverage the statistical power of large, cosmological, dark matter only (DMO) simulations. If DMO simulations are not able to resolve substructure abundance to within a factor of  $\sim 2$ , the utility of SHAM becomes question-

able. Furthermore, DMO simulations may not be reliable probes of substructure if the presence of baryons and various astrophysical processes associated with galaxy evolution significantly modify the abundance, distribution, and structure of sub-haloes. For example, the inclusion of baryons in cosmological simulations may more tightly bind sub-haloes, therefore increasing the survival time and abundance (Fiacconi et al. 2016). However, the net effect of baryonic physics on sub-haloes is not well understood. Despali & Vegetti (2016) find that the abundance of sub-haloes with peak mass  $\sim 10^{10} h^{-1} M_\odot$  is increased in the EAGLE simulation (Schaye et al. 2015), while it is decreased in the Illustris simulation (?). An enhanced destruction of dwarf galaxy mass sub-haloes ( $10^5 - 10^{10} h^{-1} M_\odot$ ) has been found in many zoom-in simulations (Read et al. 2006a,b; Brooks & Zolotov 2014; Wetzel et al. 2016). Garrison-Kimmel et al. (2017) find that the tidal field of central galaxies’ disks results in a depletion in the abundance of sub-haloes by a factor of  $\sim 2$  in the central regions compared to DMO simulations. If the inclusion of the baryonic physics of galaxy formation and evolution generically decreases the abundance of sub-haloes, this only serves to increase the small scale galaxy clustering problem in SHAM.

Given the uncertain contribution of orphan galaxies, in this paper we have also examined two other physically motivated methods to enhance the satellite contribution in mass-based SHAM models. First, we examine the effect of allowing satellite galaxies to grow in mass after accretion for some time before quenching. Within this framework, the process(es) which quenches satellites is delayed, while in the interim satellites continue to form stars similarly to central galaxies (Wetzel et al. 2013). This idea is at odds with the assumption in many SHAM models that the stellar mass of satellites is set at  $z_{\text{acc}}$  and serves as a sort of fossil record of the SMHM relation at that redshift. Continued growth after accretion generally increases the number of satellites above a given stellar mass threshold. We find that reasonable delay times before quenching result in modest increases to the satellite fraction and, as a result, the clustering signal on small scales. Again, Y12 find evidence for significant post-accretion evolution of stellar mass, such that satellites acquire a stellar mass that is close to that of central galaxies. Our model for growth allows for even larger masses, but remains insufficient. (Behroozi et al. 2015) apply a similar model for post-accretion growth and find consistent results when examining close galaxy pairs, but do not comment on  $w_p(r_p)$ . Regardless, our results suggest post-accretion evolution of satellites is an important phenomena to model in order to reproduce the small scale clustering of galaxies, but this effect on its own is not sufficient to solve the clustering crisis in this paper.

Finally, we show that galaxy assembly bias can increase clustering in mass-based SHAM models.

In this model, earlier forming (sub-)haloes host more massive galaxies. We find that such a model must contain two features. First, the strength of the galaxy assembly bias must decrease towards high mass haloes. Second, the scatter in the SMHM relation must increase towards lower masses. Both of these features maximize the effect in low mass haloes, while minimizing it in high mass haloes where there is no issue in matching clustering observations. However, we are not able to build a self-consistent evolving

- 1208 SHAM model with strong enough assembly bias to match 1268  
 1209 clustering observations. 1269  
 1210 Regardless of the method, satellite galaxies at  $z=0$  must 1270  
 1211 be more massive than central galaxies in haloes of equal peak 1271  
 1212 mass to match observations. Matching the detailed or even 1272  
 1213 aggregate stellar mass growth history of both central and 1273  
 1214 satellite galaxies may be beyond simple one (or two parameter) 1274  
 1215 SHAM (CAM) models. We speculate that a combination 1275  
 1216 of both continued stellar mass growth after accretion of 1276  
 1217 satellites and galaxy assembly bias are necessary to resolve 1277  
 1218 this crisis. 1278
- Knebe A., et al., 2011, MNRAS, 415, 2293  
 Knebe A., et al., 2013, MNRAS, 435, 1618  
 Kravtsov A. V., Klypin A. A., Khokhlov A. M., 1997, ApJS, 111,  
 73  
 Kravtsov A. V., Berlind A. A., Wechsler R. H., Klypin A. A.,  
 Gottlöber S., Allgood B., Primack J. R., 2004, ApJ, 609, 35  
 Kroupa P., 2001, MNRAS, 322, 231  
 Lehmann B. V., Mao Y.-Y., Becker M. R., Skillman S. W., Wechsler R. H., 2015  
 Li C., White S. D. M., 2009, MNRAS, 398, 2177  
 Li Y., Mo H. J., Gao L., 2008, MNRAS, 389, 1419  
 Lim S., Mo H., Lan T.-W., Ménard B., 2016  
 Lin W. P., Jing Y. P., Lin L., 2003, MNRAS, 344, 1327  
 Ludlow A. D., Navarro J. F., Springel V., Jenkins A., Frenk C. S.,  
 Helmi A., 2009, ApJ, 692, 931  
 Macciò A. V., Kang X., Fontanot F., Somerville R. S., Koposov  
 S. E., Monaco P., 2009, MNRAS, pp 1995–2008  
 Mamon G. A., Sanchis T., Salvador-Solé E., Solanes J. M., 2004,  
 A&A, 414, 445  
 Mandelbaum R., Wang W., Zu Y., White S., Henriques B., More  
 S., 2015  
 Matthee J., Schaye J., Crain R. A., Schaller M., Bower R., Theuns  
 T., 2016  
 More S., van den Bosch F. C., Cacciato M., Mo H. J., Yang X.,  
 Li R., Li R., 2009, MNRAS, 392, 801  
 More S., van den Bosch F. C., Cacciato M., Skibba R., Mo H. J.,  
 Yang X., 2011, MNRAS, 410, 210  
 Moster B. P., Somerville R. S., Maulbetsch C., van den Bosch  
 F. C., Macciò A. V., Naab T., Oser L., 2010, ApJ, 710, 903  
 Moster B. P., Naab T., White S. D. M., 2013, MNRAS, 428, 3121  
 Moustakas J., et al., 2013, ApJ, p. 50  
 Muldrew S. I., Pearce F. R., Power C., 2011, MNRAS, 410, 2617  
 Navarro J. F., Frenk C. S., White S. D. M., 1997, 490, 493  
 Onions J., et al., 2012, MNRAS, 423, 1200  
 Padmanabhan N., White M., Eisenstein D. J., 2007, MNRAS,  
 376, 1702  
 Paranjape A., Kovač K., Hartley W. G., Pahwa I., 2015  
 Pujol A., et al., 2017  
 Read J. I., Wilkinson M. I., Evans N. W., Gilmore G., Kleyna  
 J. T., 2006a, MNRAS, 366, 429  
 Read J. I., Wilkinson M. I., Evans N. W., Gilmore G., Kleyna  
 J. T., 2006b, MNRAS, 367, 387  
 Reddick R. M., Wechsler R. H., Tinker J. L., Behroozi P. S., 2013,  
 ApJ, 771, 30  
 Rees M. J., Ostriker J. P., 1977, MNRAS, 179, 541  
 Rodríguez-Puebla A., Primack J. R., Avila-Reese V., Faber S. M.,  
 2017  
 Saito S., et al., 2015  
 Sales L. V., Navarro J. F., Abadi M. G., Steinmetz M., 2007,  
 MNRAS, 379, 1475  
 Schaye J., et al., 2015, MNRAS, 446, 521  
 Sunayama T., Hearin A. P., Padmanabhan N., Leauthaud A.,  
 2015  
 The Astropy Collaboration et al., 2013, A&A, 558, A33  
 Tinker J. L., et al., 2016  
 Tomczak A. R., et al., 2014, ApJ, 783, 85  
 Vale A., Ostriker J. P., 2004, MNRAS, 353, 189  
 Wang L., Jing Y. P., 2010, MNRAS, 402, 1796  
 Wang L., Li C., Kauffmann G., De Lucia G., 2006, MNRAS, 371,  
 537  
 Watson D. F., Berlind A. A., Zentner A. R., 2012, ApJ, 754, 90  
 Watson D. F., et al., 2015, MNRAS, 446, 651  
 Wechsler R. H., Bullock J. S., Primack J. R., Kravtsov A. V.,  
 Dekel A., 2002, ApJ, 568, 52  
 Wechsler R. H., Zentner A. R., Bullock J. S., Kravtsov A. V.,  
 Allgood B., 2006, ApJ, 652, 71  
 Wetzel A. R., White M., 2010, MNRAS, 403, 1072  
 Wetzel A. R., Tinker J. L., Conroy C., 2012, MNRAS, 424, 232

## 1219 ACKNOWLEDGEMENTS

1220 FvdB is supported by the Klaus Tschira Foundation and  
 1221 by the US National Science Foundation through grant AST  
 1222 1516962.

## 1223 REFERENCES

- Baldry I. K., Glazebrook K., Driver S. P., 2008, MNRAS, 388,  
 945  
 Behroozi P. S., Conroy C., Wechsler R. H., 2010, ApJ, 717, 379  
 Behroozi P. S., Wechsler R. H., Wu H.-Y., 2013a, ApJ, 762, 109  
 Behroozi P. S., Wechsler R. H., Wu H.-Y., Busha M. T., Klypin  
 A., Primack J. R., 2013b, ApJ, 763, 18  
 Behroozi P. S., Wechsler R. H., Conroy C., 2013c, ApJ, 770, 57  
 Behroozi P. S., Wechsler R. H., Lu Y., Hahn O., Busha M. T.,  
 Klypin A., Primack J. R., 2014a, ApJ, 787, 156  
 Behroozi P. S., Wechsler R. H., Lu Y., Hahn O., Busha M. T.,  
 Klypin A., Primack J. R., 2014b, ApJ, 787, 156  
 Behroozi P. S., et al., 2015  
 Bell E. F., McIntosh D. H., Katz N., Weinberg M. D., 2003, ApJS,  
 149, 289  
 Blanton M. R., Roweis S., 2007, AJ, 133, 734  
 Borch A., et al., 2006, A&A, 453, 869  
 Brooks A. M., Zolotov A., 2014, ApJ, 786, 87  
 Bryan G. L., Norman M. L., 1998, ApJ, 495, 80  
 Chabrier G., 2003, The Publications of the Astronomical Society  
 of the Pacific, 115, 763  
 Conroy C., Wechsler R. H., 2009, ApJ, 696, 620  
 Conroy C., Wechsler R. H., Kravtsov A. V., 2006, ApJ, 647, 201  
 Desmond H., Wechsler R. H., 2015, MNRAS, 454, 322  
 Despali G., Veggetti S., 2016, arXiv, p. arXiv:1608.06938  
 Fall S. M., Efstathiou G., 1980, MNRAS, 193, 189  
 Fiacconi D., Madau P., Potter D., Stadel J., 2016, ApJ, 824, 144  
 Gao L., White S. D. M., 2007, Monthly Notices of the Royal  
 Astronomical Society: Letters, 377, L5  
 Gao L., Springel V., White S. D. M., 2005, Monthly Notices of  
 the Royal Astronomical Society: Letters, 363, L66  
 Garrison-Kimmel S., et al., 2017  
 Gill S. P. D., Knebe A., Gibson B. K., 2005, MNRAS, 356, 1327  
 Guo Q., White S., 2013, MNRAS, 437, 3228  
 Guo Q., Guo Q., White S., White S., Li C., Boylan-Kolchin M.,  
 2010, MNRAS, 404, 1111  
 Hearin A. P., Watson D. F., 2013, MNRAS, 435, 1313  
 Hearin A. P., Zentner A. R., Berlind A. A., Newman J. A., 2013,  
 MNRAS, 433, 659  
 Hearin A. P., Watson D. F., Becker M. R., Reyes R., Berlind  
 A. A., Zentner A. R., 2014, MNRAS, 444, 729  
 Hearin A., et al., 2016  
 Hu W., Kravtsov A. V., 2003, ApJ, 584, 702  
 Jiang F., van den Bosch F. C., 2016, MNRAS, 458, 2848  
 Klypin A. A., Trujillo-Gomez S., Primack J., 2011, ApJ, 740, 102

- 1336 Wetzel A. R., Tinker J. L., Conroy C., van den Bosch F. C., 2013, 1388  
 1337 MNRAS, 432, 336 1389
- 1338 Wetzel A. R., Tinker J. L., Conroy C., van den Bosch F. C., 2014, 1390  
 1339 MNRAS, 439, 2687
- 1340 Wetzel A. R., Hopkins P. F., Kim J.-h., Faucher-Giguere C.-A., 1390  
 1341 Kereš D., Quataert E., 2016, ApJ, p. L23
- 1342 White S. D. M., Rees M. J., 1978, MNRAS, 183, 341 1391
- 1343 Yang X., Mo H. J., van den Bosch F. C., 2003, MNRAS, 339, 1392  
 1344 1057 1393
- 1345 Yang X., Mo H. J., van den Bosch F. C., Zhang Y., Han J., 2012, 1394  
 1346 ApJ, 752, 41 1395
- 1347 Yang X., Mo H. J., van den Bosch F. C., Bonaca A., Li S., Lu Y., 1396  
 1348 Lu Y., Lu Z., 2013, ApJ, 770, 115 1397
- 1349 Zentner A. R., Hearn A. P., van den Bosch F. C., 2014, MNRAS, 1398  
 1350 443, 3044
- 1351 Zu Y., Mandelbaum R., 2015b 1399
- 1352 Zu Y., Mandelbaum R., 2015a 1400
- 1353 van Uitert E., et al., 2016, MNRAS, 459, 3251 1401
- 1354 van den Bosch F. C., 2016
- 1355 van den Bosch F. C., Jiang F., 2014
- 1356 van den Bosch F. C., Jiang F., 2016, MNRAS, 458, 2870 1402
- 1357 van den Bosch F. C., Yang X., Mo H. J., 2003, MNRAS, 340, 771 1403
- 1358 van den Bosch F. C., et al., 2007, MNRAS, 376, 841 1404
- 1359 van den Bosch F. C., Aquino D., Yang X., Mo H. J., Pasquali A., 1404  
 1360 McIntosh D. H., Weinmann S. M., Kang X., 2008, MNRAS, 1405  
 1361 387, 79 1406
- 1362 van den Bosch F. C., More S., Cacciato M., Mo H., Yang X., 2013, 1407  
 1363 MNRAS, 430, 725 1408
- 1364 van den Bosch F. C., Jiang F., Hearn A., Campbell D., Watson 1409  
 1365 D., Padmanabhan N., 2014, MNRAS, 445, 1713 1410
- 1366 van den Bosch F. C., Jiang F., Campbell D., Behroozi P., 2016, 1411  
 1367 MNRAS, 455, 158 1412

## APPENDIX A: HALO PROPERTIES

1368 In this section we describe how we calculate properties for  
 1369 (sub-)haloes which depend on their growth history. We use  
 1370 the merger trees constructed using the **Consistent** trees al-  
 1371 gorithm (Behroozi et al. 2013b) built on the **ROCKSTAR** halo  
 1372 catalogues from the Bolshoi simulation. We distinguish be-  
 1373 tween host-haloes and sub-haloes using the **upid** tag for each  
 1374 halo. If **upid**  $\equiv -1$ , a halo is considered a host; otherwise,  
 1375 if **upid**  $> 0$ , we consider it a sub-halo. For this work, we do  
 1376 not distinguish between higher order sub-haloes (i.e. sub-  
 1377 sub-haloes). 1378

### A1 Peak Halo Mass

1379 We use the peak halo mass obtained by each (sub-)halo to  
 1380 assign stellar mass in each of the models discussed in this  
 1381 paper. We calculate the peak mass,  $\widetilde{M}_{\text{peak}}$ , a (sub-)halo at  
 1382  $z=0$  obtained throughout its history while not identified as  
 1383 a sub-halo as:

$$\widetilde{M}_{\text{peak}} = \text{MAX}[m'_{\text{vir}}(z)]$$

1385 where,

$$m'_{\text{vir}}(z) = \begin{cases} m_{\text{vir}}(z) & \text{if host-halo at } z \\ 0.0 & \text{if sub-halo at } z \end{cases} \quad (\text{A2})$$

1386 We then define  $z_{\text{peak}}$  as the redshift where  $m'_{\text{vir}}(z_{\text{peak}}) \equiv$   
 1387  $\widetilde{M}_{\text{peak}}$ . This differs from the typical definition of peak halo

mass which does not require the peak mass to be obtained while a halo is identified as a host-halo:

$$M_{\text{peak}} = \text{MAX}[m_{\text{vir}}(z)] \quad (\text{A3})$$

The former definition,  $\widetilde{M}_{\text{peak}}$ , disregards any mass growth which occurs while a halo is identified as a sub-halo. We prefer  $\widetilde{M}_{\text{peak}}$  as a physical parameter because most growth that occurs while a halo is identified as a sub-halo is most often a numerical artifact. However, we do note that we ignore the rare case of subhalo-subhalo mergers. In Fig. A1 we show the growth histories for three haloes in the Bolshoi simulation. In each panel, we also show the running  $\widetilde{M}_{\text{peak}}(z)$  and mark the redshift where  $\widetilde{M}_{\text{peak}}$  is reached. In the right hand panel we show a case where  $\widetilde{M}_{\text{peak}} \neq M_{\text{peak}}$  for a halo which briefly ‘grows’ in mass after accretion. We find this is the case for  $\sim 10\%$  of sub-haloes.

### A2 Halo Accretion Time

The purpose of this section is to define a “primary” accretion redshift,  $z_{\text{acc,prim}}$ , which is most important for galaxy evolution. Each of the evolving models in this work require a single accretion redshift for all sub-haloes, where it is assumed that the stellar mass of satellites is set at the time of accretion, or where a special post-accretion growth regime begins. However, a halo may undergo many accretion events throughout its history. This makes the identification of a single, most important, accretion redshift non-trivial.

With this in mind, we define the accretion redshift of a halo as the redshift at which it is first identified as a sub-halo after having been first identified as a host-halo<sup>6</sup>. Furthermore, because a sub-halo’s orbit may take it beyond the virial radius of its host (e.g. backsplash haloes), it is possible to identify multiple accretion redshifts for many haloes. Given this, we define  $z_{\text{acc,n}}$  as the redshift a halo is identified as a sub-halo for the  $n^{\text{th}}$  time. We also tabulate ‘ejection’ redshifts,  $z_{\text{ej},n}$ , the redshift a halo is identified as being a host-halo after previously having been identified as a sub-halo for the  $n^{\text{th}}$  time. As an example, in the middle panel of Fig. A1, we show the growth history of a halo which underwent three accretion events and two ejections since  $z \sim 6$ .

We explore four definitions for  $z_{\text{acc,prim}}$ :

- (i) the highest accretion redshift,  $z_{\text{acc,1}}$ ,
- (ii) the most recent  $z_{\text{acc,n}}$ ,
- (iii) the highest accretion redshift that is not followed by a continuous period of more than two dynamical times as a host-halo before being re-accreted (or reaching  $z=0$ ),
- (iv) and the highest accretion redshift that occurs after  $z_{\text{peak}}$ .

The first definition for  $z_{\text{acc,prim}}$  we examine is  $z_{\text{acc,1}}$ . We can eliminate this as a viable definition because we find that a significant fraction of host-haloes at  $z \sim 0$  were briefly identified as a sub-halo at high redshifts. An example is shown in the left hand panel of Fig. A1. We find that between 4% and 10% of haloes more massive than  $10^{12} h^{-1} M_{\odot}$  have  $z_{\text{acc,1}}$  and  $z_{\text{ej},1} > 3$  and remain a host-halo up to  $z \sim 0$ . It is

<sup>6</sup> For the rare case of ‘immaculate’ sub-haloes, sub-haloes with no progenitor (van den Bosch 2016), we use the first redshift for which the halo is identified.

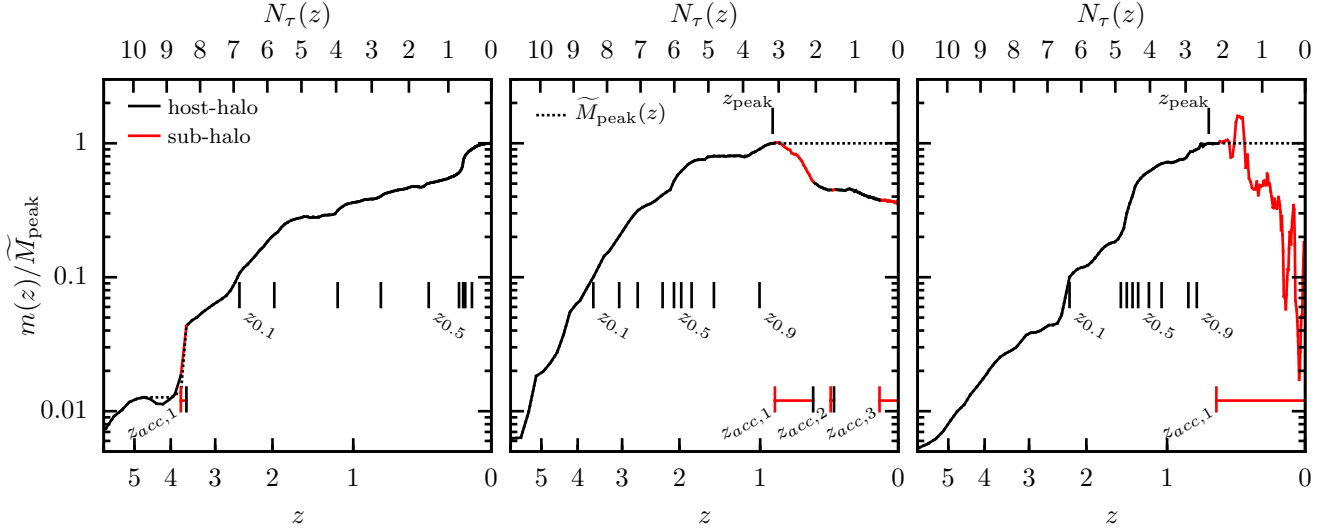


**Figure A1.** As an example, we show the mass growth histories for three haloes, all with a peak mass of  $\sim 10^{12} h^{-1} M_{\odot}$ . When a halo is identified as a host-halo ( $\text{upid} \equiv -1$ )  $m_{\text{vir}}(z)/\tilde{M}_{\text{peak}}$  is shown as a solid black line. When a halo is identified as a sub-halo ( $\text{upid} > 0$ )  $m_{\text{vir}}(z)/\tilde{M}_{\text{peak}}$  is shown as a solid red line. A series of formation times,  $z_f = [0.1, 0.2, \dots, 0.9]$  are marked as vertical black dashes below the growth histories. Similarly,  $z_{\text{peak}}$  is marked above the growth histories. At the bottom of each panel, any accretion redshifts are shown as a red vertical dash connected to the associated ejection redshift marked with a black vertical dash (or through  $z=0$  if it remains a sub-halo). The running peak mass,  $\tilde{M}_{\text{peak}}(z)$ , is plotted as a dotted black line. The upper x-axis in each panel is the number of dynamical times until  $z=0$  from eq. A4.

clear that these haloes should be treated more as traditional host haloes than haloes that host satellite galaxies.

The second definition we consider for  $z_{\text{acc,prim}}$  is the most recent accretion redshift. This definition suffers the same problem as the previous by assigning too many host-haloes a high redshift  $z_{\text{acc,prim}}$ . In addition, such a definition ignores the accretion history of backsplash haloes by only considering the most recent accretion event. Up to 60% of sub-haloes are on orbits whose apocenter is beyond the virial radius of their effective host-halo, and around  $\sim 10\%$  of accreted sub-structure is found beyond the virial radius of their associated host-halo at  $z \sim 0$  (Lin et al. 2003; Gill et al. 2005; Sales et al. 2007; Ludlow et al. 2009; Wetzel et al. 2014; van den Bosch 2016). The middle panel of Fig. A1 shows an example of a halo which was accreted and ejected multiple times in line with the expectation for backsplash haloes.

To address both spurious high-redshift accretions and backsplash haloes at lower redshift, we consider a third definition for  $z_{\text{acc,prim}}$  that takes into account the amount of time a halo remains a host-halo after being ejected. For backsplash haloes, the time-scale for re-accretion will be on the order of dynamical time. If a halo remains a host-halo for much more time, evolution as a typical host-halo is more likely as in the case of host-haloes which were briefly identified as a sub-halo at high-redshift.

To this end, we calculate the number of dynamical times elapsed between redshift  $z$  and 0 as:

$$N_{\tau}(z) = \int_0^{t(z)} \frac{dt}{\tau_{\text{dyn}}(t)} \quad (\text{A4})$$

where  $\tau_{\text{dyn}}$  is the dynamical time given by:

$$\begin{aligned} \tau_{\text{dyn}}(t) &= \sqrt{\frac{3\pi}{16G\bar{\rho}_h(z)}} \\ &= 1.628 h^{-1} \text{Gyr} \left[ \frac{\Delta_{\text{vir}}(z)}{178} \right] \left[ \frac{H(z)}{H_0} \right]^{-1} \end{aligned} \quad (\text{A5})$$

where  $\bar{\rho}_h(z)$  is the average density of a virialized dark matter halo at redshift  $z$ . The number of dynamical times between the  $i^{\text{th}}$  ejection and the  $i+1^{\text{th}}$  accretion is then given by:

$$\Delta N_{\tau} = N_{\tau}(z_{\text{ejt},i}) - N_{\tau}(z_{\text{acc},i+1}) \quad (\text{A6})$$

For any accretion redshift which is not followed by a continuous time,  $\Delta N_{\tau}$ , as a host-halo, we mark as the primary accretion redshift. For haloes that remain a host for  $\Delta N_{\tau}$  after being ejected, we disregard the previous accretion events when defining  $z_{\text{acc,prim}}$ . We find that  $\Delta N_{\tau} = 2$  is a good threshold to separate backsplash-ing sub-haloes and host-haloes with spurious high redshift accretion events.

The final definition for the primary accretion redshift we explore is the highest redshift accretion that occurs after  $\tilde{M}_{\text{peak}}$ . This naturally removes any prior accretion events that were followed by mass growth while also generally picking out the initial accretion redshift for haloes that backsplash. This definition lines up with  $z_{\text{acc},1}$  in the middle and right-hand panels of Fig. A1. We also find that  $z_{\text{acc,prim}}$  defined using the last two definitions (iii, iv) are different in less than 2% of haloes with mass greater than  $10^{12} h^{-1} M_{\odot}$ . Given the simplicity of this definition, we adopt this as our fiducial  $z_{\text{acc,prim}}$  in the rest of this paper and simply refer to it as  $z_{\text{acc}}$ .

We show the effect on clustering for different definitions

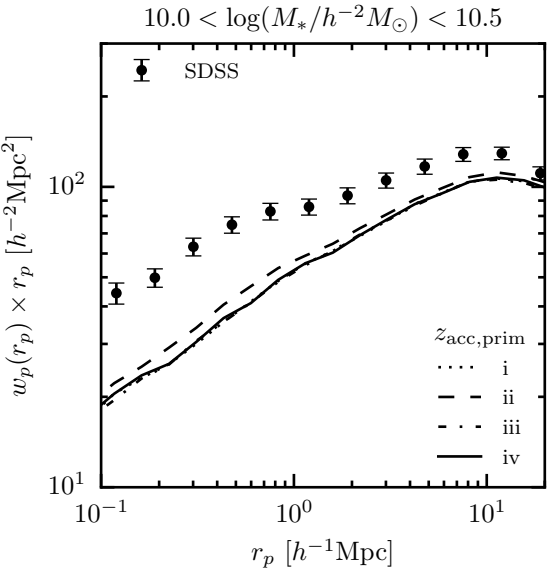


**Figure A2.** Similar to Fig. 12, a comparison of the effect of different definitions of  $z_{\text{acc,prim}}$  on  $w_p(r_p)$  in the M13 model. The model predictions for different  $z_{\text{acc,prim}}$  definitions are shown as lines of various styles corresponding to the definitions listed in Appendix A2. The lines for definitions i, iii, and iv fall nearly on-top of each other.

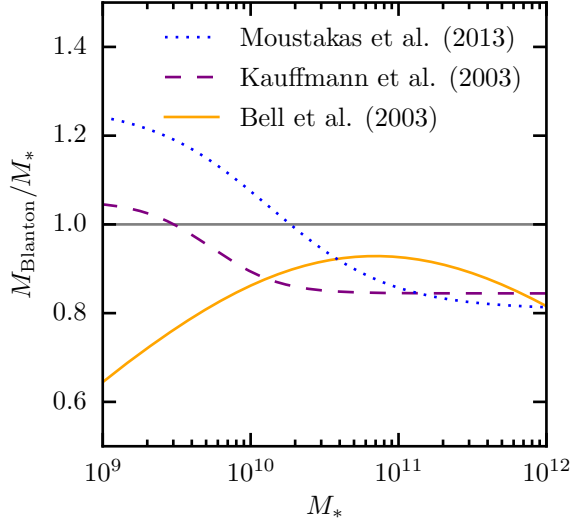


**Figure B1.** mass conversion between Blanton stellar masses and the other stellar mass systems used in this paper.

of  $z_{\text{acc,prim}}$  for the M13 model in Fig. A2. The only significant difference is between the last accretion redshift (definition ii) and the others (i, iii, iv). Using the last accretion redshift results in satellites with larger stellar masses relative to the other definitions as a result of the evolution in the SMHM relation towards larger stellar masses at fixed halo mass as  $z \rightarrow 0$ . Satellites that are ejected get a boost in stellar mass relative to those that remain satellites. We consider this an unappealing model for satellite evolution.

### A3 Halo Formation Time

We calculate the formation time of a halo,  $z_f$ , as the redshift at which a halo is first identified as exceeding a mass larger than or equal to  $f \times \bar{M}_{\text{peak}}$  while not identified as a sub-halo. In Fig. A1 we show  $z_f$  for  $f=0.1, 0.2, \dots, 0.9$  for three different halo growth histories marked with short vertical dashes below  $m_{\text{vir}}(z)$  in each panel.

## APPENDIX B: STELLAR MASS CONVERSIONS

Each of the evolving models in this paper (M13, B13, and Y12) was tuned to fit stellar mass functions based on different methods to measure  $M_*$ . In order to facilitate comparisons between models, we apply a set of simple conversion to correct for the mean difference in order to make the stellar masses more consistent with the Blanton & Roweis (2007) stellar masses,  $M_{\text{Blanton}}$ , used in LW09 and the RM and RV models. A summary of these functions is shown in Fig. B1.

Here we describe in detail each of these conversions. M13 fits to the LW09 stellar mass function at  $z \sim 0$  which was modified based on a conversion suggested by Guo et al. (2010) which transforms the stellar masses based on the SDSS r-band Petrosian magnitudes to ones based on SDSS r-band model magnitudes. We undo this modification by reducing the stellar masses in M13 by 10%. B13 fits to the Baldry et al. (2008) and Moustakas et al. (2013) mass functions at  $z < 0.2$ . The Baldry et al. (2008) stellar masses are an average of many different techniques which makes a simple conversion prescription difficult. On the other hand, Moustakas et al. (2013) provide a comparison between masses derived using the iSEDfit and the Blanton & Roweis (2007) masses. We find the the mean difference is well fit by:

$$\log(M_{\text{Blanton}}/M_{\text{iSEDfit}}) = a_1 + a_2 \tanh\left(\frac{M_{\text{iSEDfit}} - a_3}{a_4}\right) \quad (\text{B1})$$

where  $a_1 = 0.0056$ ,  $a_2 = -0.098$ ,  $a_3 = 10.53$ , and  $a_4 = 0.82$ . We transform the B13 masses using this relation and find satisfactory results. The Y12 model uses stellar masses based on the technique of Bell et al. (2003) assuming a universal IMF (Kroupa 2001; Borch et al. 2006). We use the inverse of the transformation between Bell et al. (2003) and Blanton & Roweis (2007) masses provided in Appendix A in LW09:

$$\log(M_{\text{Bell}}/M_{\text{Blanton}}) = a_1 + a_2 M_{\text{Blanton}} + a_3 M_{\text{Blanton}}^2 + a_3 M_{\text{Blanton}}^3 + a_3 M_{\text{Blanton}}^4 \quad (\text{B2})$$

where  $a_1 = 2.0$ ,  $a_2 = -0.043$ ,  $a_3 = -0.045$ ,  $a_4 = 0.0032$ , and  $a_5 = -2.1 \times 10^{-5}$ .

## APPENDIX C: ORPHAN GALAXIES

We define “orphan” galaxies as satellites in our mock galaxy catalogues which have no identified sub-halo. Our implementation of abundance matching requires a halo or sub-halo be associated with each galaxy. In order to add the flexibility of including a population of orphan galaxies, we post-process the halo catalogues, adding “clone” sub-haloes that are made available to host orphan galaxies.

To generate a clone, we randomly draw from the list of all sub-haloes to choose a “donor” sub-halo. The clone sub-halo receives all the properties of the donor sub-halo (e.g.  $z_{\text{acc}}$ ) except its phase space coordinates and those properties associated with its host-halo. A new host-halo is chosen for the clone by randomly choosing a host-halo with a mass close to that of the donor’s host ( $\pm 0.1$  dex). We apply two methods to assign a new set of phase space coordinates to the clone:

(i) maintaining the relative position,  $\Delta \vec{x}$ , and velocity,  $\Delta \vec{v}$ , between a clone’s host-halo as in the donor’s host-halo (**sub-profile**),

(ii) assigning the phase-space coordinates of a randomly selected particle belonging to the clone’s host to the clone (**dm-profile**).

For the former method, we use the positions and velocities of host-haloes and sub-haloes from the ROCKSTAR halo catalogue. For the later, we use a down-sampled catalogue of dark matter particles consisting of  $\sim 1\%$  of all particles to facilitate computational ease. We assign particles to host-haloes by finding all particles within a distance  $r_{\text{vir}}$  of each host. When a particle can be assigned to more than one host under this condition, we assign the particle to the nearest host-halo. After this process, we find that  $\sim 1\%$  of clones occupy a host-halo with no associated particles (in our down-sampled catalogue). In this small fraction of cases, we revert to the first method.

Each of these methods has merits. The first method acts under the assumption that the sub-haloes that host orphan galaxies (and missing from the available halo catalogues) are a fair sampling of all sub-haloes. These clones will have the same radial profile as typical sub-haloes within host-haloes of equivalent mass. The second method results in a more centrally concentrated population of orphans, one that also naturally follows the shape of the host-halo. This may be a more appropriate if the majority of orphans occupy sub-haloes that are missing because they are hard to identify in the dense central regions of host-haloes or highly evolved sub-haloes which have sunk to the central regions of their host-halo. Neither of these methods will preserve sub-halo-sub-halo correlations. In particular, neither of these methods specifically deals with higher-order sub-haloes, e.g. sub-sub-haloes, and treats all sub-haloes regardless of order the same in the cloning process. To help with visualization of each of these methods, we plot the position of sub-haloes and clones in Fig. C1 for both methods. In the bottom panel, one can see that the clones are more centrally concentrated than both the extant sub-haloes and clones assigned positions maintaining the relative distance to the host-halo centre.

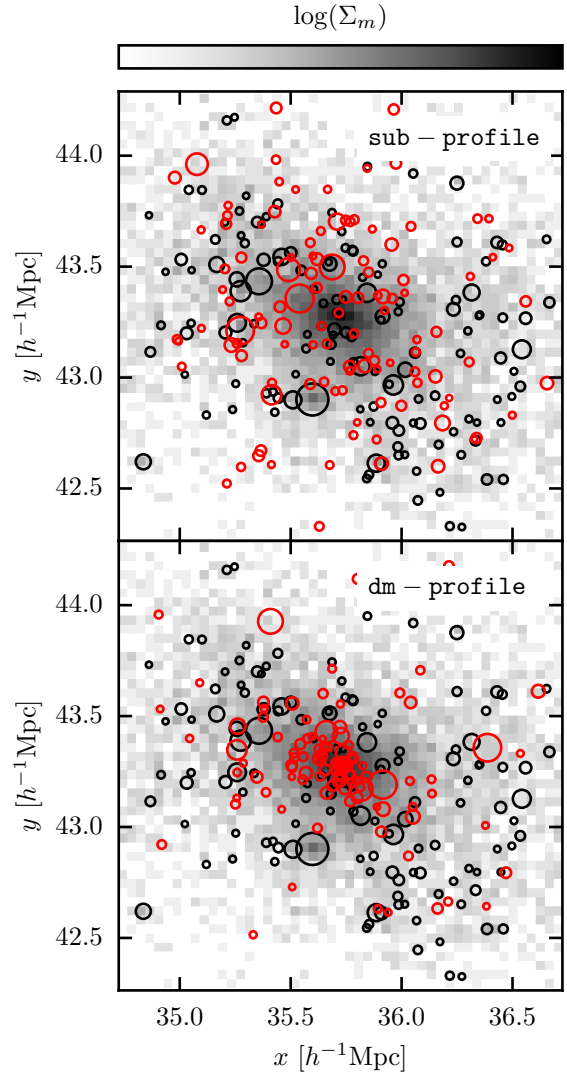


**Figure C1.** The projected distribution of sub-haloes with  $M_{\text{peak}} > 10^{11} h^{-1} M_{\odot}$  (black circles) for an example host-halo ( $m_{\text{vir}} \simeq 10^{14} h^{-1} M_{\odot}$ ), where the projected density of dark matter is shown in grey-scale (the same in upper and lower panels). In addition, the upper panel shows clone sub-haloes (red circles) where the relative distance and velocity with respect to the centre of mass is preserved (**sub-profile**). The bottom panel shows clone sub-haloes where the position and velocity is assigned by drawing random particles from the host-halo (**dm-profile**). The size of the circles is proportional to the viral radius at peak mass,  $r_{\text{vir}}(z_{\text{peak}})$ , of each sub-halo.

## APPENDIX D: DEGRADING RANK ORDER CORRELATIONS

Given two variables,  $X$  and  $Y$ , that form finite data sets, e.g.  $x_1, x_2, \dots, x_n$ , of length  $n$ , the correlation between the variables can be characterized by the Spearman’s rank order correlation coefficient:

$$\rho_{XY} = 1 - \frac{6 \sum d_i^2}{n(n^2 - 1)} \quad (\text{D1})$$

1604 where  $d_i$  is the difference in ranks of  $x_i$  and  $y_i$ :

$$d_i = n_i^x - n_i^y \quad (\text{D2})$$

1605 For example, if  $X$  and  $Y$  are both in rank order, e.g.  $n_1^x = 1, n_2^x = 2, \dots, n_n^x = n$ , then  $\rho_{XY} = 1.0$ .

1606 Here we describe an algorithm to degrade the ordering  
1607 of two variables,  $X$  and  $Y$ , each of length  $n$ . To begin with  
1608 a positive correlation, each variable is placed in rank order:

$$\begin{aligned} X' &= \text{RANK}(X, X) \\ Y' &= \text{RANK}(Y, Y) \end{aligned} \quad (\text{D3})$$

1610 where the  $\text{RANK}(A, B)$  operator sorts  $A$  by the rank order  
1611 values of  $B$ . It should be noted that to begin with a negative  
1612 correlation between  $X$  and  $Y$ ,  $X'$  would be put in inverse  
1613 rank order, i.e.  $X' = \text{RANK}(X, -X)$ . Next, a new variable,  
1614  $Q$ , is calculated for  $X'$  from the ranks by adding a normal  
1615 random variable to each rank:

$$q_i = n_i^{x'} + \mathcal{N}(0, \sigma_q \times n) \quad (\text{D4})$$

1616 where  $\sigma_q$  is approximately the standard deviation of the  
1617 change in the order relative to the length of  $n$ .  $X'$  can then  
1618 be re-ordered by  $Q$ :

$$X'' = \text{RANK}(X', Q) \quad (\text{D5})$$

1619 Henceforth, we will refer to these two variables with trans-  
1620 formed ordering simply as  $X$  and  $Y$ .

1621 This method is inherently random in nature, and given  
1622 a value of  $\sigma_q$ , the rank order correlation between  $X$  and  $Y$   
1623 will vary depending on the size of the data sets. In Fig. D1  
1624 we examined the relation between the correlation coefficient,  
1625  $\rho_{XY}$ , and  $\sigma_q$  for two uniform random variables of length  
1626  $n = 10^3$ . For each value of  $\sigma_q$  we repeat the process described  
1627 above 100 times. The error bars in Fig. D1 are the standard  
1628 deviation in  $\rho_{XY}$  from these 100 realizations. From this, we  
1629 derive the relation between  $\langle \rho_{XY} \rangle$  and  $\sigma_q$ , and we use this  
1630 relation to choose  $\sigma_q$  for a desired value of  $\rho_{XY}$ . We provide  
1631 an accurate fitting function for the relation given by:

$$\langle \rho_{XY} \rangle(\sigma_q) = 1 - f(\sigma_q) \quad (\text{D6})$$

$$f(x) = \frac{1}{2} e^{-\left(\frac{x}{x_1}\right)^\alpha} + \frac{1}{2} \left[ 1 + \left(\frac{x}{x_2}\right)^\beta \right]^{-1}$$

1632 where  $x_1 = 2/3$ ,  $x_2 = 0.3$ ,  $\alpha = -1$ , and  $\beta = -2$ . Further-  
1633 more, this relation is independent of the size of  $X$  and  $Y$   
1634 and is not affected by the distribution of values themselves  
1635 since it is based on the rank ordering.

## 1636 APPENDIX E: ADDING SCATTER TO THE 1637 SMHM RELATION

1638 This paper has been typeset from a TeX/LaTeX file prepared by  
1639 the author.

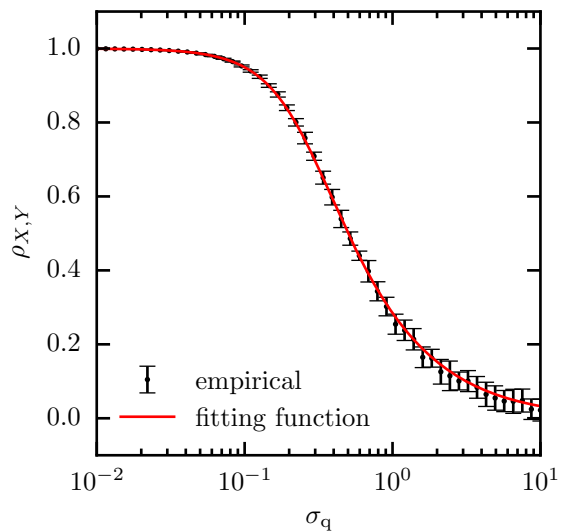


**Figure D1.** The relation between rank scatter parameter,  $\sigma_q$ , and the Spearman's correlation coefficient,  $\rho$ . The fitting function, eq. D6, is shown as a red line.